RSC Advances

PAPER

View Article Online
View Journal | View Issue

Cite this: *RSC Adv.*, 2022, **12**, 33032

Design, synthesis, theoretical study, antioxidant, and anticholinesterase activities of new pyrazolo-fused phenanthrolines†

Efraín Polo-Cuadrado, *[a] Cristian Rojas-Peña,[ab] Karen Acosta-Quiroga,[ab] Lorena Camargo-Ayala,[c] Iván Brito, [d] Jonathan Cisterna,[d] Félix Moncada,[e] Jorge Trilleras, [f] Yeray A. Rodríguez-Núñez [g] and Margarita Gutierrez *[a]

Pyrazole-fused phenanthroline compounds were obtained through several synthetic routes. NMR, HRMS, and IR techniques were used to characterize and confirm the chemical structures. Crystal structures were obtained from compounds **3a**, **5b**, **5j**, **5k**, and **5n** and analyzed using X-ray diffraction. Compounds were evaluated as acetyl (AChE) and butyrylcholinesterase (BChE) inhibitors, and the results showed a moderate activity. Compound **5c** presented the best activity against AChE (IC_{50} = 53.29 μM) and compound **5l** against BChE enzyme (IC_{50} = 119.3 μM). Furthermore, the ability of the synthetic compounds to scavenge cationic radicals DPPH and ABTS was evaluated. Compound **5e** (EC_{50} = 26.71 μg mL^{-1}) presented the best results in the DPPH assay, and compounds **5e**, **5f** and **5g** (EC_{50} = 11.51, 3.10 and <3 μg mL^{-1}, respectively) showed better ABTS cationic radical scavenging results. Finally, *in silico* analyses indicated that 71% of the compounds show good oral availability and are within the ranges established by the Lipinski criteria.

Received 2nd September 2022
Accepted 3rd November 2022

DOI: 10.1039/d2ra05532e

rsc.li/rsc-advances

1. Introduction

Many compounds of interest in the pharmacological field usually contain 5 and 6-membered heteroatom rings with nitrogen, sulfur, or oxygen atoms. The synthesis of fused heterocycles offers new opportunities to create compounds with improved biological activity and has significant relevance in medicinal chemistry.[1,2] Within this context, fused heterocycles such as pyrazolo[3,4-*b*]pyridine have been reported as antimicrobial,[3] anti-inflammatory,[4] cytotoxic,[5] and antitumoral[6] compounds. Likewise, phenanthroline derivatives have chemotherapeutic, antimicrobial, and anticancer potential, highly valued biological activities in pharmacology.[4,5,7–9]

There are various synthetic strategies for obtaining a phenanthroline scaffold. One strategy is the formation of the pyridine ring from an existing aminopyrazole in reaction with a dicarbonyl species or equivalents and aldehydes through a Hantzsch-type reaction.[10–12]

Similarly, the reaction can be initiated from a pyridine precursor that has a leaving group in the C-2 position, and an electrophilic group (carbonyl or cyano group) in the C-3 position

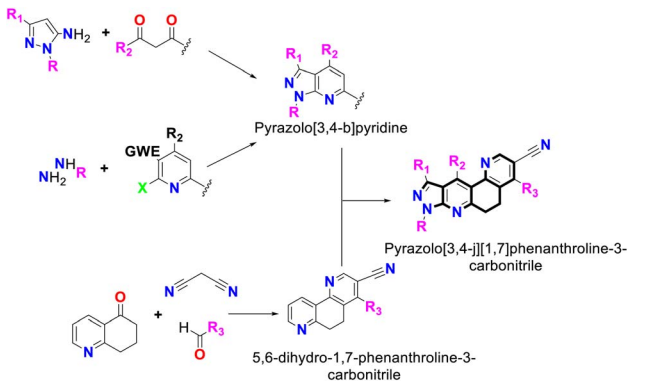

Fig. 1 Synthesis of pyrazolo[3,4-*b*]pyridine-6,8-dihydro-1,7-phenanthroline and its combined-fused derivatives.

[a]*Laboratorio Síntesis Orgánica y Actividad Biológica (LSO-Act-Bio), Instituto de Química de Recursos Naturales, Universidad de Talca, Casilla 747, Talca 3460000, Chile. E-mail: epolo@utalca.cl; mgutierrez@utalca.cl*

[b]*Doctorado en Química, Departamento de Química Orgánica y Fisicoquímica, Universidad de Chile, Santiago, Chile*

[c]*Doctorado en Ciencias Mención I + D de Productos Bioactivos, Instituto de Química de Recursos Naturales, Laboratorio de Síntesis Orgánica (LSO-Act-Bio), Universidad de Talca, Casilla 747, Talca 3460000, Chile*

[d]*Departamento de Química, Facultad de Ciencias Básicas, Universidad de Antofagasta, Avda., Campus Coloso, Antofagasta 02800, Chile*

[e]*Departamento de Química, Universidad Nacional de Colombia, Av. Cra 30 # 45-03, Bogotá, Colombia*

[f]*Grupo de Investigación en Compuestos Heterocíclicos, Universidad del Atlántico, Puerto Colombia 081007, Colombia*

[g]*Departamento de Química, Facultad de Ciencias Exactas, Universidad Andrés Bello, Republica 275, Santiago, 8370146, Chile*

† Electronic supplementary information (ESI) available. CCDC 2200163–2200166 and 2203148. For ESI and crystallographic data in CIF or other electronic format see DOI: https://doi.org/10.1039/d2ra05532e

that a hydrazine hydrate can attack to form the fused five-membered pyrazole ring (see Fig. 1).[13]

On the other hand, phenanthrolines can be synthesized using the classic Skraup reaction from nitroanilines and glycerol in a strongly acid medium.[14] The phenanthroline derivatives[1–4,6,7,15] have been reported as scaffolds for the preparation of biologically active metal complexes.[16–18] Likewise, its 5,6-dihydro phenanthrolinic analogs are of chemical interest and can be obtained through a Michael-type addition reaction among a dihydro-5-quinolinone system, malononitrile and diverse aldehydes.[19]

Compounds derived from pyrazolo[3,4-*b*]pyridine and phenanthroline have demonstrated promising inhibitory capacity against cholinesterase enzymes (ChEs) involved in Alzheimer disease (AD) development and antioxidant capacities (AO).[20–24] In recent years, replacement therapies with AO drugs have been evaluated and investigated and have shown significant potential to reduce the symptoms and incidence of AD, characterized by a progressive deterioration of cognitive functions.[25]

One of the characteristics described in patients with AD is the accumulation of extracellular plaques of the β-amyloid peptide (Aβ), and the neurofibrillary tangles of the hyperphosphorylated tau protein.[26,27] This reduces the number of functional monomers and contributes to the loss of homeostasis of metal ions.[28,29] Furthermore, it has been found that Aβ can generate free radicals that have been strongly correlated with episodes of oxidative stress and neurotoxicity,[28,30,31] which has generated a growing interest in the relationship between oxidative stress and neurodegenerative diseases.

Likewise, it is known that with physiological aging the production of radicals or highly oxidizing species increases, and the protection capacity against these species decreases, which generates an increase in an oxidative cellular environment.[32] Several studies have been able to link increased brain oxidative stress with cognitive decline caused by normal aging and neurodegenerative diseases.[19,33] Oxidative species contribute to neuronal damage in various dementia diseases, including AD, in which oxidative damage is one of the first markers of cognitive dysfunction.[34–36]

Thus, the present work aimed to synthesize and evaluate the inhibition capacity toward the AChE and BChE enzymes and the AO capacity of a new group of compounds derived from the pyrazolo-fused phenanthroline system, in addition to computationally analyzing their pharmacokinetic properties.

2. Results and discussion

2.1 Chemistry

Initially, compound **5a** was synthesized by method A, which consisted of two continuous steps with a possible mechanism displayed in Scheme 2. Here, reagents **1a** and **2** combine to generate the (*E*)-6-benzylidene-3-methyl-1-phenyl-1,6,7,8-tetrahydro-5*H*-pyrazole[3,4-*b*]quinolin-5-one chalcone (**3a**),[37] which reacts with ammonium acetate to produce the respective imine, and subsequently undergoes a Michael-type reaction with malononitrile to produce compound **8**. This was followed by cyclization, isomerization, and aromatization to generate the final product (**5a**) in low yield (7%). Therefore, the mechanism suggests that compound **5a** was obtained by domino reactions.[38]

To obtain better yields, method B was proposed (see Scheme 3A), which, like method A, consisted of two successive stages. A possible mechanism for this method begins with a Knoevenagel reaction between an aromatic aldehyde (**1a–m**) and malononitrile (**4**), using L-proline as the catalyst, which in its zwitterion form extracts the proton of **4**, forming the respective carbanion (**4′**), which then attacks the protonated aldehyde (**1′**), forming the corresponding intermediate (**1″**) that loses water to produce molecule **13** (see Scheme 3B).[39] Simultaneously, compound **2** reacts with ammonium acetate to produce imine **11**, which by isomerization is transformed into enamine **12**, which subsequently undergoes a Michael reaction with compound **13** to produce molecule **14**, which by isomerization transforms into compound **8**, which after cyclization, isomerization and aromatization generates the final product **5a–m** with yields of up to 59%.[38] Structurally, these final compounds have a 2-amino-3-cyanoquinoline system that is of great interest for both reactivity and biological applications. Analogues to this system have been obtained through ionic liquid assisted synthesis,[40] which may be used as an alternative synthetic strategy in future works.

Finally, method C was used to obtain compounds **5n–p**. In Scheme 4, a possible reaction mechanism is proposed for this method, which, like the previous two, consisted of two successive stages. Initially, a Knoevenagel reaction occurs between the aromatic aldehyde (**1n–p**) and malononitrile **4**, using L-proline as a catalyst to produce molecule **13**, in the same way as in methodology B (see Scheme 3B). Simultaneously, compound **2** reacts with sodium hydride to produce the enolate **15**, which undergoes a Michael reaction with compound **13** to produce molecule **16**. This molecule is cyclized, and by the action of ethanol in the medium compound **17** is formed, which undergoes dehydration and finally aromatization to generate compound **5n–p**.[41]

On the other hand, to provide relevant information when characterizing the type of phenanthrolines obtained in this work, the vibrational frequencies of molecules **5a** and **5p** were calculated computationally and compared with those obtained experimentally by infrared spectroscopy. Molecules **5a** and **5p** are selected because molecule **5a** is the base structure of phenanthrolines **5a–m**, while **5p** is the base structure of compounds **5n–p**.

2.2 FT-IR spectra

Experimental and simulated (B3LYP/6-31G*) infrared (IR) spectra of molecules **5a** and **5p** are shown in Fig. 2. The resulting vibrational frequencies for the optimized geometries, the proposed vibrational assignments, and the IR intensities are given in Table 1. The modes are numbered from the lowest to highest frequency. Comparisons of theoretical and experimental IR spectra indicate that strong vibrations in the experimental spectrum are also strong in the theoretical spectrum.

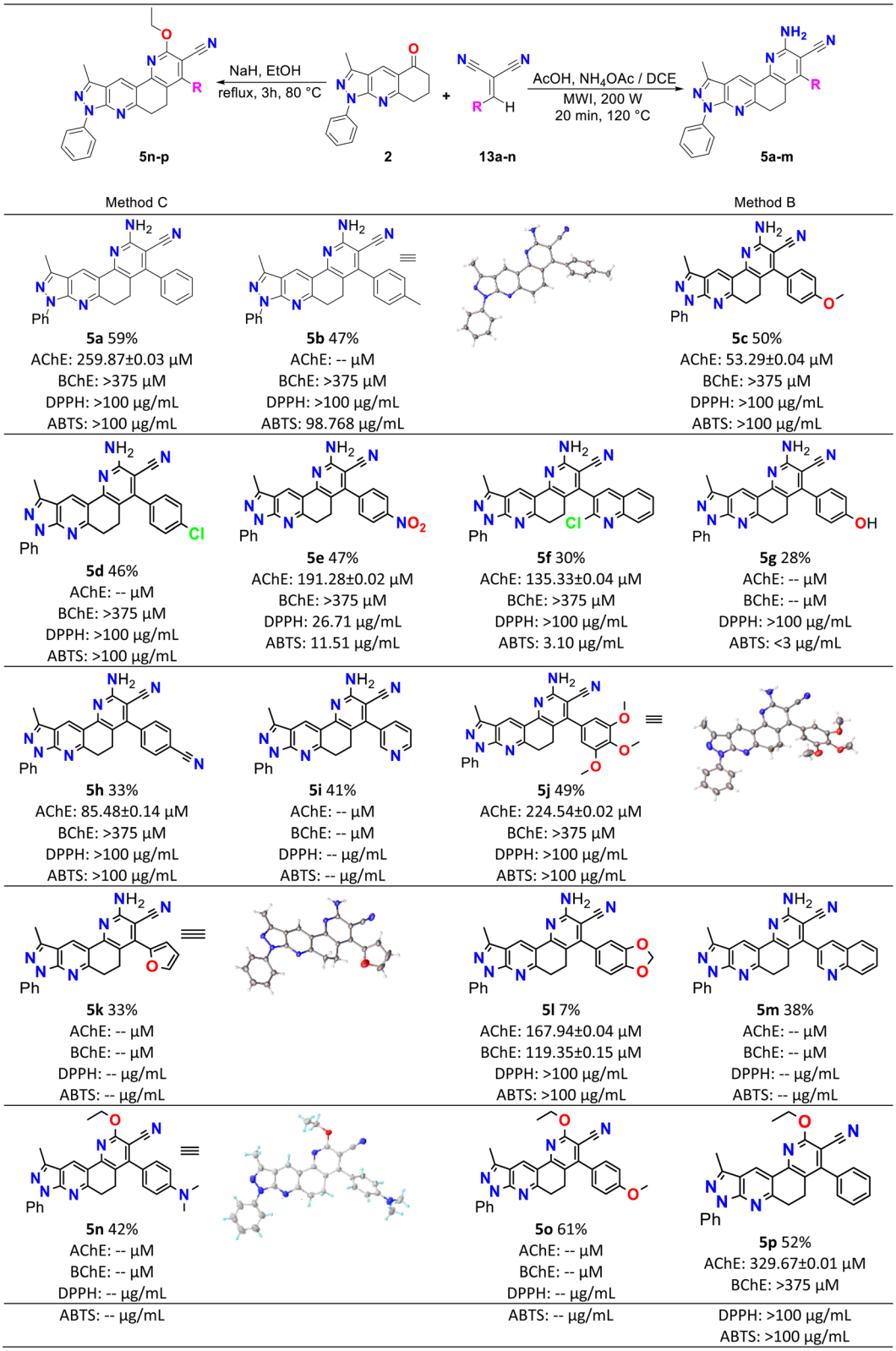

Scheme 1 Synthesis, yields, biological and antioxidant activities of pyrazolo[3,4-*j*][1,7]phenanthroline-3-carbonitrile derivatives (**5a–p**).

As seen in Table 1, there are some useful strong frequencies in the IR to characterize the **5a** and **5p** molecules, along with their respective derivatives, such as the C=C stretching band, around 1600 cm^{-1}. The nitrile stretching (Csp–N) was observed around 2210 cm^{-1}, while the symmetric stretching of methylene (Csp3–H) was observed at about 2905 cm^{-1}. On the other hand,

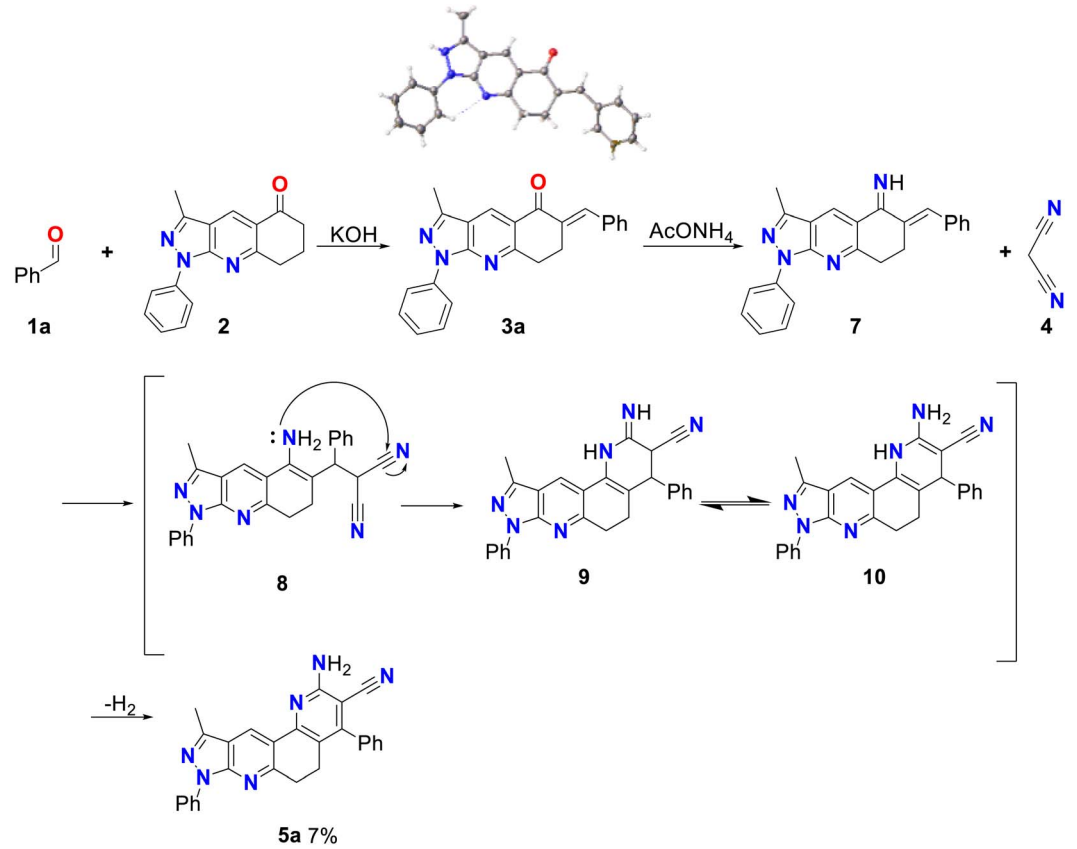

Scheme 2 Mechanism by method A of 2-amino-10-methyl-4,8-diphenyl-6,8-dihydro-5*H*-pyrazolo[3,4-*j*][1,7]phenanthroline-3-carbonitrile (**5a**).

the symmetric stretching of methyl (Csp3–H) and the Csp2–H stretching were observed at about 3080 cm^{-1}.

In addition, bands are observed for fundamental frequencies in identifying the **5a** molecule and its derivatives, such as the amine (N–H) snipping signal at 1610 cm^{-1}. The N–H symmetrical stretching signal was seen at approximately 3334 cm^{-1}, and the asymmetric stretching signal of N–H at about 3427 cm^{-1}. Likewise, there are important frequencies for identifying the **5p** molecule and its derivatives, such as the alkyl ether (O–C) tension signal at 1146 cm^{-1} and the alkyl vinyl ether (C–O–C=) tension signal at 1174 cm^{-1}.

As can be seen in Table 1, the frequencies calculated with the B3LYP/6-31G*method presented a good agreement with the experimental data. Therefore this computational method is a helpful tool for the structural characterization of the compounds studied.[42]

2.3 Biological activity

Table 2 shows the results of the biological activity tests. The values obtained in the anticholinesterase tests were expressed as half of the maximum inhibitory concentration (IC_{50}). The results reveal that most of the analyzed compounds presented inhibitory activity of ChEs enzymes. IC_{50} values were between 53.29 and 329.67 μM for AChE and between 119.3 and >875.17 μM for BChE. Among the compounds synthesized, **5c** (IC_{50} = 53.29 μM) presented the best inhibitory activity against AChE; however, its potency was lower than that of the positive control galantamine (IC_{50} = 0.57 μM). Furthermore, **5l** presented the best inhibition result against the BChE enzyme, with an IC_{50} = 119.3 μM that was 15 times less potent than galantamine (IC_{50} = 8.08 μM).

Molecular docking was used to understand the binding mode of compound **5c**, which presented the best inhibitory activity against AChE. As observed in Fig. 3, the ligand did not present any interaction with constituent residues of the active site and, due to its rigidity, it does not fully enter the catalytic cavity, being located at approximately 8 Å from the catalytic triad (residues in yellow). It is found by obstructing access to the stabilized pocket through an aromatic hydrogen bond type interaction between residue D276 and a hydrogen from the phenol ring linked to the pyrazole scaffold. This interaction is observed at the periphery of the active site cavity and is energetically weaker than a classical hydrogen bond.

Similarly, the results of the antioxidant tests were reported as the mean maximum effective concentration (EC_{50}). The results show that all the analyzed compounds presented antioxidant activity in the tests carried out (DPPH and ABTS). The EC_{50} ranges obtained were 26.71 and >100 μg mL^{-1} for the DPPH assay and <3 and >100 μg mL^{-1} for the ABTS assay. Among the

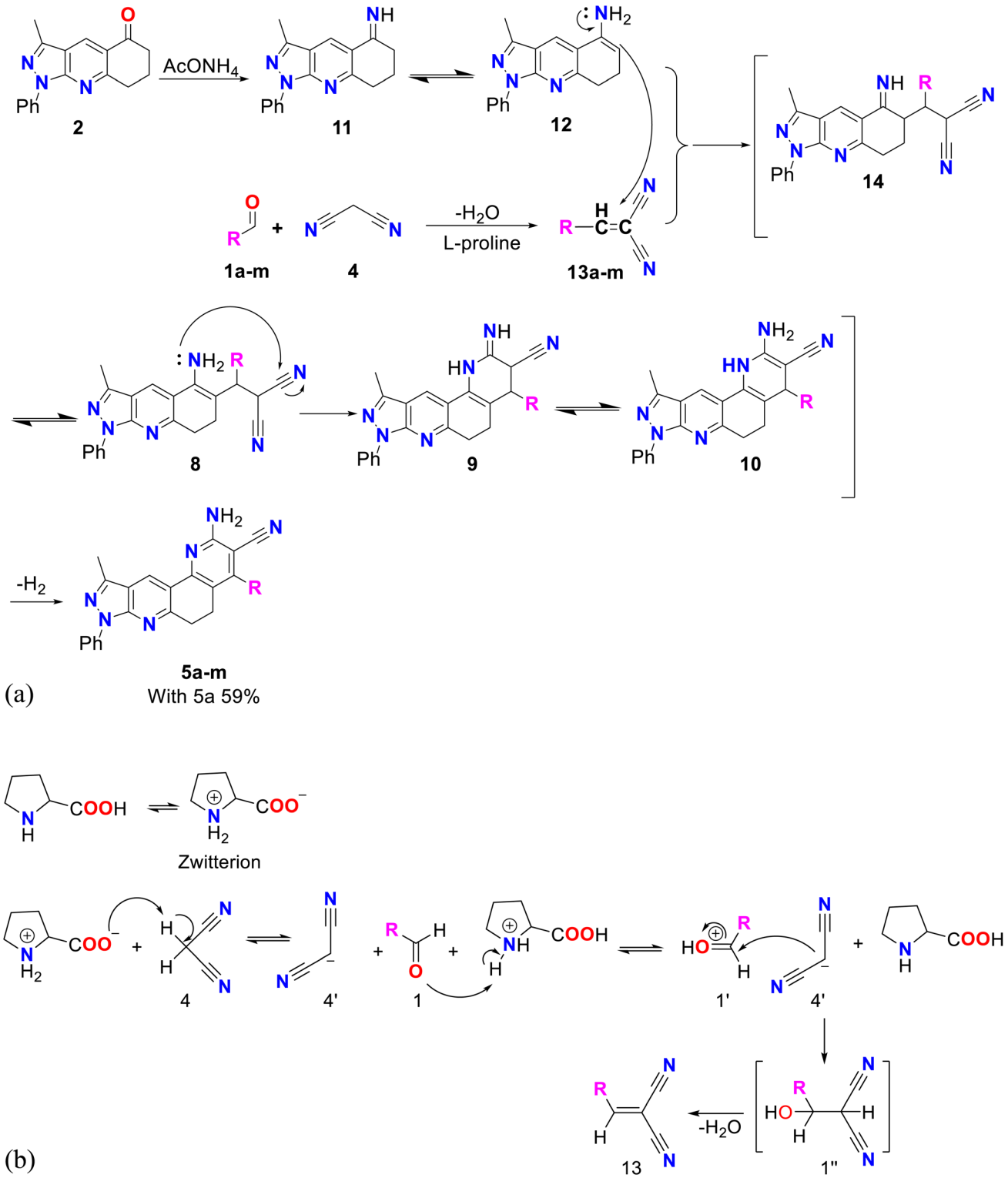

Scheme 3 (A) Mechanism by method B of pyrazolo[3,4-*j*][1,7]phenanthroline-3-carbonitrile (**5a–m**). (B) Mechanism of Knoevenagel reaction catalyzed by L-proline.

compounds analyzed, **5e** (EC_{50} = 26.71 μg mL^{-1}) presented better results in the DPPH test. However, its antioxidant potency did not exceed that of ascorbic acid (EC_{50} = 1.5 μg mL^{-1}), used as a positive control. Compounds **5e**, **5f**, and **5g** (see Scheme 1) presented EC_{50} values of 11.51, 3.10, and <3 μg mL^{-1}, respectively, in the ABTS test, being more effective in stabilizing the ABTS radical 2, 9 and more than nine times compared to ascorbic acid (EC_{50} = 27.62 μg mL^{-1}).

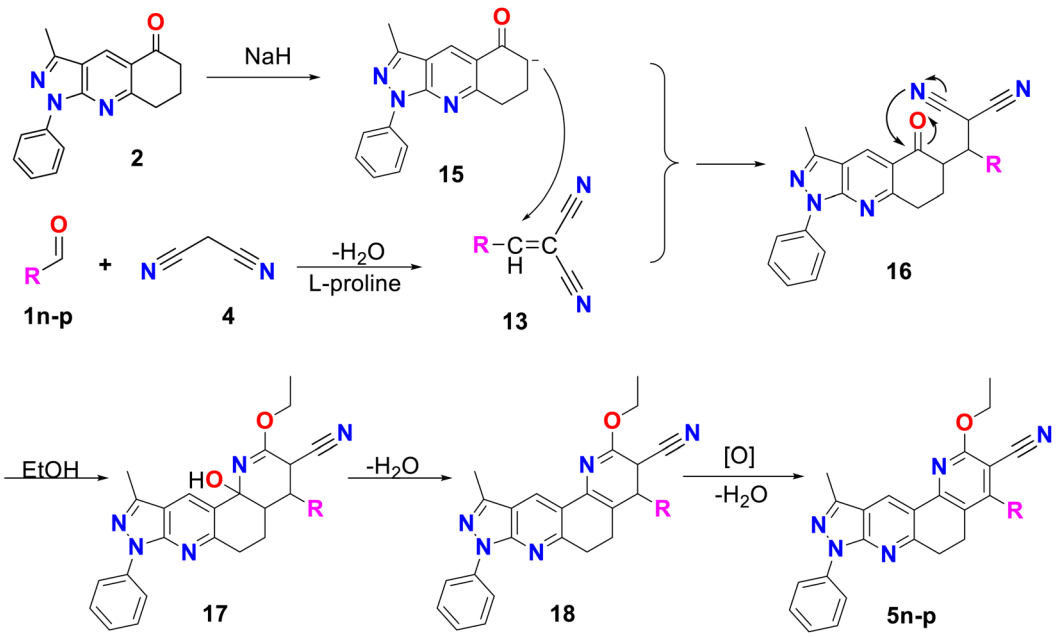

Scheme 4 Mechanism by method C of pyrazolo[3,4-*j*][1,7]phenanthroline-3-carbonitrile derivatives (**5n–p**).

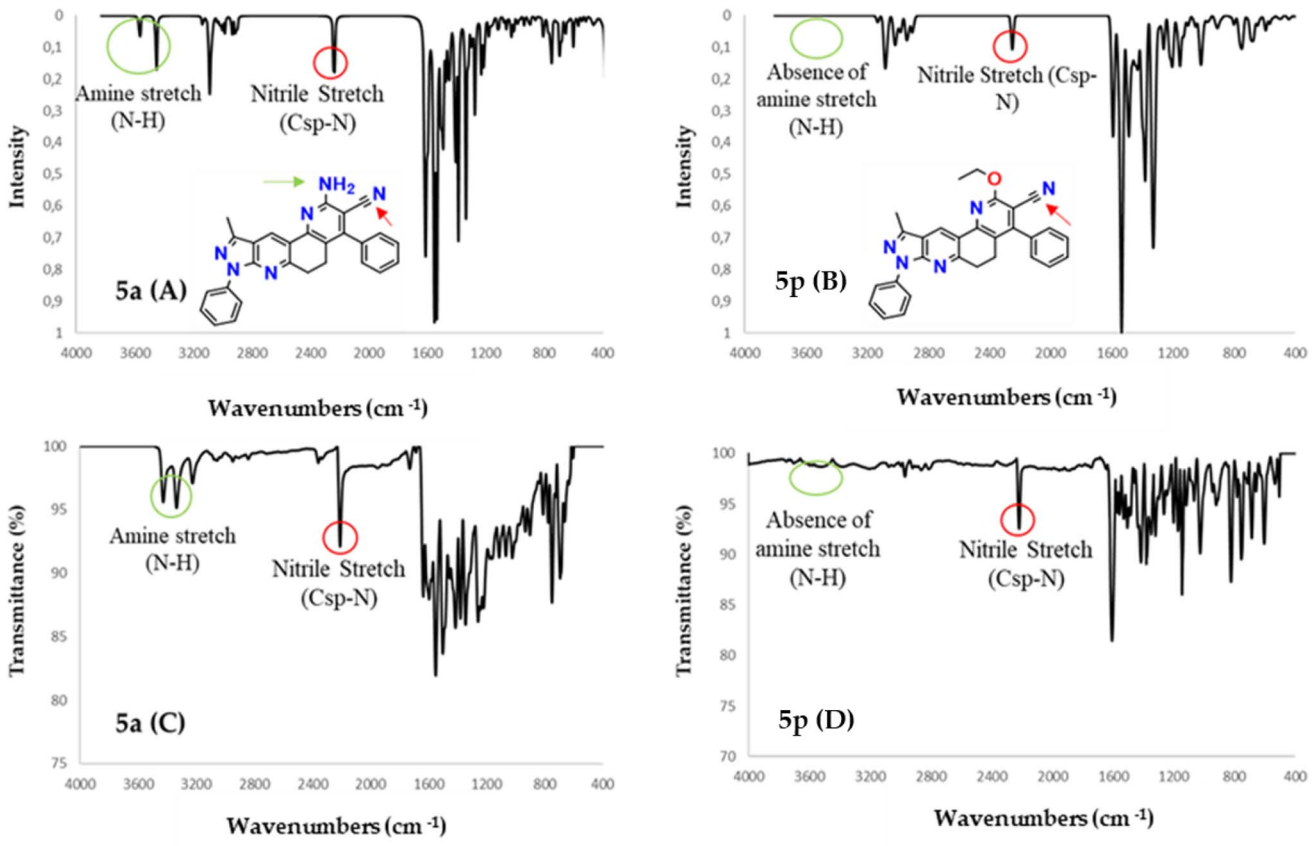

Fig. 2 IR spectra calculated with DFT (B3LYP/6-31G*) (A and B) along with experimental (C and D) IR spectra for molecules **5a** and **5p**.

Both ABTS and DPPH radicals can be stabilized by hydrogen atom transfer (HAT) or electron transfer (ET) mechanisms, but the reactivity patterns and mechanism are difficult to interpret.[43] With these considerations, it is possible to infer that the antioxidant activity presented by the compounds is due to the presence of nitrogen atoms, which can act on radicals

Table 1 Comparison of calculated and experimental vibration spectra (FT-IR) of compounds **5a** and **5p**

	B3LYP/6-31G(d)	Experimental in this study		
Normal mode	Freq[a] (cm^{-1})	Intensity (km mol^{-1})	Freq (cm^{-1})	Approximate assignments
5a				
1	1033	0.93	1034	Balancing methyl (C–H)
2	1450	7.73	1452	Methyl twist (C–H)
3	1386	143.00	1346	Methyl symmetric bending (C–H)
4	1457	0.01	1466	Scissoring methylene (C–H)
5	1533	201.84	1593	Stretch C–C
6	1606	354.99	1610	Scissor amine (N–H)
7	2229	114.71	2210	Nitrile stretch (Csp–N)
8	2890	9.78	2898	Asymmetric stretching methylene (C–H)
9	2903	29.20	2908	Symmetric stretching methylene (C–H)
10	2927	24.77	2941	Symmetrical stretching methyl (C–H)
11	2975	15.05	2979	Asymmetric methyl stretching (C–H)
12	3081	42.14	3078	Alkene stretch (Csp2–H)
13	3445	74.54	3334	Symmetric stretching amine (N–H)
14	3559	35.48	3427	Asymmetric stretching amine (N–H)
5p				
1	1019	33.43	1026	Balancing methyl (C–H)
2	1155	63.7	1146	Tension alkyl ether C–O
3	1202	79.2	1174	Tension alkyl vinyl ether C–O–C=
4	1327	170.4	1321	Methyl symmetric bending (C–H)
5	1533	455.77	1606	Stretch C=C
6	2251	62.2	2217	Nitrile stretch (Csp–N)
7	2906	27.99	2908	Symmetric stretching methylene (C–H)
8	2944	19.51	2966	Symmetrical stretching methyl (C–H)
9	3081	41.96	3074	Alkene stretch (Csp2–H)

[a] Scaling factor: 0.963.

Table 2 Antioxidant and acetyl and butyrylcholinesterase inhibitory activities of compounds

	Anticholinesterase assay		Antioxidant assay		
Compound	AChE[a] (μM)	BChE[a] (μM)	DPPH[b] (μg mL^{-1})	ABTS[b] (μg mL^{-1})	Fold[e]
5a	259.87 ± 0.03	>875.17	>100	>100	—
5b	nd	>847.41	>100	98.77	0.28
5c	53.29 ± 0.04	>817.84	>100	>100	—
5d	nd	>810.04	>100	>100	—
5e	191.28 ± 0.015	≥375	26.71	11.51	2.40
5f	135.33 ± 0.04	≥375	>100	3.10	8.91
5g	nd	nd	>100	<3	
5h	85.48 ± 0.14	≥375	>100	>100	—
5i	nd	nd	nd	nd	—
5j	224.54 ± 0.018	≥375	>100	>100	—
5k	nd	nd	nd	nd	—
5l	167.94 ± 0.04	119.35 ± 0.15	>100	>100	—
5m	nd	nd	nd	nd	—
5n	nd	nd	nd	nd	—
5o	nd	nd	nd	nd	—
5p	329.67 ± 0.01	≥375	>100	>100	—
Galantamine[c]	0.57 ± 0.05	8.08 ± 0.02	—	—	—
Ascorbic acid[d]	—	—	1.5 ± 0.2	27.62 ± 3.5	1

[a] IC_{50} ± SEM. [b] EC_{50}. [c] Reference compound of the anticholinesterase assay. [d] Reference compound of the antioxidant assay. [e] Fold = IC_{50} of ascorbic acid/IC_{50} of compounds **5a–p**.

through ET. The "NH_2" groups present in compounds **5a–k** can contribute to stabilizing both radicals through both mechanisms.[44]

On the other hand, the results for molecules **5e**, and **5f** in the ABTS test could be mainly attributed to the presence of the substituents "4-NO_2 and 2-chloroquinoline", respectively. The

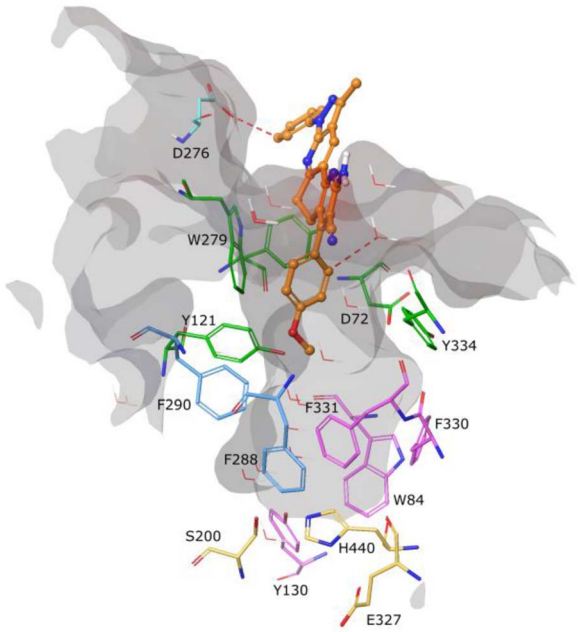

Fig. 3 Binding molecular interactions for compound **5c** (faded orange) within AChE active sites. Residues of AChE are shown in stick representation. Catalytic triad (yellow), peripheral anionic (orange), anionic site (magenta), and oxyanion hole (blue). Red dotted lines represent aromatic H-bonds. Relevant amino acids are shown in a thin tube. Compound **5c** is shown in ball-and-stick representation. The active site cavity is represented in gray.

presence of electron withdrawing groups such as "Cl" and "NO_2" has been shown to improve the antioxidant activity of the molecules that contain them.[45] In contrast, the molecules that contain electron donor groups such as "Me" or "OMe" tend to impair the antioxidant capacity, which could justify the results for molecules **5e**, **5c**, **5j**, and **5k**. Compounds containing quinoline rings have been reported to have significant antioxidant properties, especially if these quinolines contain halogen atoms.[46–48]

Furthermore, some secondary metabolites are phenolic compounds, whose natural function is to act as antioxidants for plants.[49] Numerous studies show that compounds containing phenolic rings tend to show results comparable to or better than positive controls such as ascorbic acid.[50–53] It has even been reported that there is a direct relationship between the number of free hydroxyl groups of phenolic compounds and their antioxidant activity, and it has been reported that the position of said hydroxyl groups in aromatic rings also plays an important role in antioxidant capacity.[50,53] The good results presented by compound **5g** suggest considering further studies to analyze the influence of the number and position of the free hydroxyl group in the phenolic ring on the antioxidant capacity of pyrazolophenanthroline derivatives.

Physicochemical properties and drug-likeness (Lipinski's rules[54]), along with gastrointestinal absorption and brain permeability (Table S1 and Fig. S48†), of the synthesized compounds were determined using the open access software SwissADME (**https://www.swissadme.ch**).[55] The ranges exhibited by the synthesized compounds for each of the parameters that make up Lipinski's criteria are molecular weight M_W values (<500) from 428.49 to 518.57, hydrogen bond donor HBD (<5) from 0 to 2, hydrogen bond acceptor HBA (<10) from 4 to 7 and log *P* (<5) from 3.10 to 4.79. Fig. 4 shows the drug-likeness distribution graphs of synthesized compounds. Thus, 82% of the compounds did not violate Lipinski's rules, and the rest of them only showed one violation corresponding to M_W above the established range. Likewise, 71% of the compounds presented high gastrointestinal absorption, while none of them presented permeability of the blood–brain barrier. It is important to highlight that compound **5f** is not a substrate for P-glycoprotein (P-gp), which could indicate that its bioavailability would not be reduced (Fig. S1†). According to the biological results presented, the compounds obtained are biologically active and promising to be used as oral drugs.

DFT calculations were performed for compounds **5a–p** to better understand the relationship between their structure and their antioxidant activity. Table S2† displays the HOMO and LUMO energies obtained from those calculations along with the computed electronegativity, chemical hardness, smoothness, and electronic affinity. The results obtained from the computational analysis show that molecule **5e** presents the highest LUMO energy, electronic affinity, softness and electronegativity. The first three properties provide information on the ease to accept electrons of a compound along with its susceptibility to nucleophilic attacks. In addition, it has been shown that molecules with high electronegativity display high antioxidant capacity as they tend to form stable radical species. These results are consistent with the biological assays since the **5e** molecule presented the best values in the DPPH test and was one of the three molecules that presented antioxidant capacity exceeding the ABTS test positive control. The significant correlation between the electronic properties evaluated and the antioxidant capacity for the **5e** molecule suggests that the interaction with the studied radicals is through electronic transfer. No other correlation between the electronic properties and the antioxidant activities was observed.

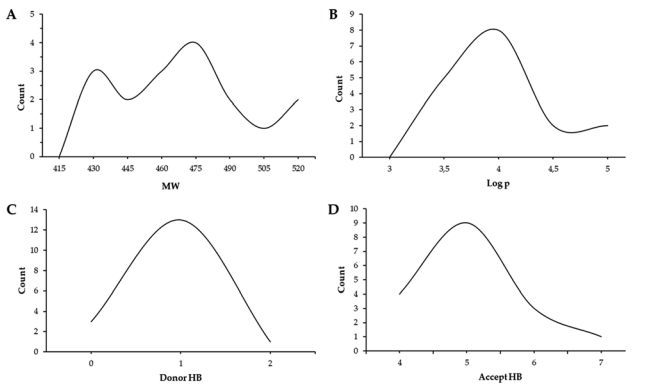

Fig. 4 Distribution graphs of synthesized compounds' molecular properties.

2.4 X-Ray diffraction measurements

Suitable diffraction-quality single crystals for X-ray structural studies were obtained for compounds **3a**, **5b**, **5j**, **5k** and **5n**. All compounds crystallize in centrosymmetric space groups (see Table 3 for more details). Molecular and crystal structures of each compound are displayed in Fig. 5. All compounds show normal bond angles and distances.[56]

Additionally, crystal data are summarized in Table 3, while selected bond distances and angles, as well as intra- and intermolecular hydrogen bonds, are provided in Tables 4 and 5. The molecular structure of compound **3a** corresponds to three-fused rings of 3-methyl-1*H*-pyrazole (3MP), and 4,5,6,7,8-tetrahydro-5-quinolinone (THQ) moieties with benzyl and phenyl groups attached to the THQ and 3MP rings, respectively. Meanwhile, the compounds **5b**, **5j**, **5k**, and **5n** are four-fused rings composed of 3MP and functionalized 5,6-dihydro-1,7-phenanthroline (DHPhen), with tolyl (**5b**), 1-(2,3,4-trimethoxy) phenyl (**5j**), furyl (**5k**), and 1-(4-*N*,*N*′-aminomethyl)phenyl (**5n**) groups (see Fig. 5 for more details).

All compounds show dihedral angles between phenyl and fused 3MP rings. The values of these dihedral angles are 20.22(9), 11.45(9), 12.19(11), and 1.84(14)°, respectively. In compound **5n**, this small value is caused by an intramolecular hydrogen bond between the phenyl and the fused pyridyl ring, the latter being an almost coplanar fragment.

In the case of compound **3a**, this shows a dihedral angle of 44.85(12)° between the benzyl group and the THQ ring. Additionally, all compounds show dihedral angles between their respective substituent ring, and fused DPH in ring of 57.25(9), 73.70(8), 133.25(12)/68.0(9), and 121.18(13)° for **5b**, **5j**, **5k**, and **5n**, respectively. Additionally the saturated six-membered ring has two different conformations, according to Cremer & Pople parameters.[57] In the cases of compounds **3a**, **5j**, **5k**, and **5n** this conformation is screw-boat, and in the case of compound **5b** is twist-boat (see Table 4 for more details).

In the crystal structure, the molecules in each compound are stabilized by intra- and intermolecular hydrogen bond interactions C–H···N, C–H···O, and N–H···N. The details of these interactions are depicted in Table 5. In compounds **5b**, and **5k** N–H···N interactions generate a supramolecular 2D aggregate with base vectors [0 1 0], and [2 0 1], and plane (1 0–2); meanwhile, in compounds **5j** and **5n**, C–H···N, and N–H···N generate

Table 3 X–ray crystallographic data and structural refinement for compounds **3a**, **5b**, **5j**, **5k** and **5n**

Compound	**3a**	**5b**	**5j**	**5k**	**5n**
Empirical formula	$C_{24}H_{19}N_3O$	$C_{28}H_{22}N_6$	$C_{30}H_{26}N_6O_3$	$C_{25}H_{18}N_6O$	$C_{31}H_{28}N_6O$
Formula mass, g mol^{-1}	365.42	442.51	518.57	418.45	500.59
CCDC	2200163	2200166	2200164	2200165	2203148
Collection *T*, K	296.49	296.86	295.94	296.33	294.94
Crystal system	Monoclinic	Monoclinic	Monoclinic	Monoclinic	Triclinic
Space group	$P2_1/c$	$P2_1/c$	$P2_1/n$	$P2_1/c$	$P\bar{1}$
a (Å)	14.714(2)	10.4257(14)	10.0883(8)	11.971(14)	8.156(2)
b (Å)	16.279(3)	13.8104(17)	12.4670(11)	14.236(19)	9.356(2)
c (Å)	7.7182(12)	16.570(2)	20.6411(18)	12.823(15)	19.728(5)
α (°)	90	90	90	90	101.682(5)
β (°)	94.980(2)	101.663(3)	100.785(2)	101.08(4)	92.413(5)
γ (°)	90	90	90	90	114.101(5)
V (Å^3)	1841.8(5)	2336.6(5)	2550.2(4)	2144(5)	1332.6(6)
Z	4	4	4	4	2
ρ_{calcd} (g cm^{-3})	1.318	1.258	1.351	1.296	1.248
Crystal size (mm)	0.19 × 0.15 × 0.12	0.21 × 0.18 × 0.15	0.18 × 0.16 × 0.11	0.17 × 0.15 × 0.10	0.17 × 0.15 × 0.09
F(000)	768.0	928.0	1088.0	872.0	528.0
Abs coeff (mm^{-1})	0.082	0.078	0.090	0.084	0.079
2*θ* range (°)	17.8 to 59.458	5.746 to 52.09	5.892 to 54.016	5.724 to 56.056	5.616 to 53.064
Range h,k,l	−20/20, −22/22, −10/10	−12/12, −16/17, −20/20	−12/11, −15/15, −26/26	−15/15, −18/18, −16/16	−10/10, −11/10, −24/24
No. total refl.	29 908	18 109	25 717	20 098	25 207
No. unique refl.	5043	4602	5498	5099	5509
Comp. θ_{max} (%)	94.5	99.9	99.8	99.5	99.7
Max/min transmission	0.746/0.676	0.7453/0.6121	0.7454/0.6773	0.7457/0.6316	0.7454/0.6337
Data/restraints/parameters	5043/0/254	4602/0/336	5498/0/323	5099/0/295	5509/3/376
Final *R* [$I > 2\sigma(I)$]	$R_1 = 0.0665$ $wR_2 = 0.1614$	$R_1 = 0.0604$ $wR_2 = 0.1327$	$R_1 = 0.0574$ $wR_2 = 0.1366$	$R_1 = 0.0810$, $wR_2 = 0.2074$	$R_1 = 0.0797$ $wR_2 = 0.2035$
R Indices (all data)	$R_1 = 0.1016$ $wR_2 = 0.1941$	$R_1 = 0.0963$ $wR_2 = 0.1641$	$R_1 = 0.0913$ $wR_2 = 0.1633$	$R_1 = 0.1335$ $wR_2 = 0.2649$	$R_1 = 0.1508$ $wR_2 = 0.2631$
Goodness of fit/F^2	1.073	1.053	1.035	1.053	1.014
Largest diff. Peak/hole (eÅ^{-3})	0.36/−0.46	0.40/−0.26	0.45/−0.30	1.15/−0.63	0.26/−0.27

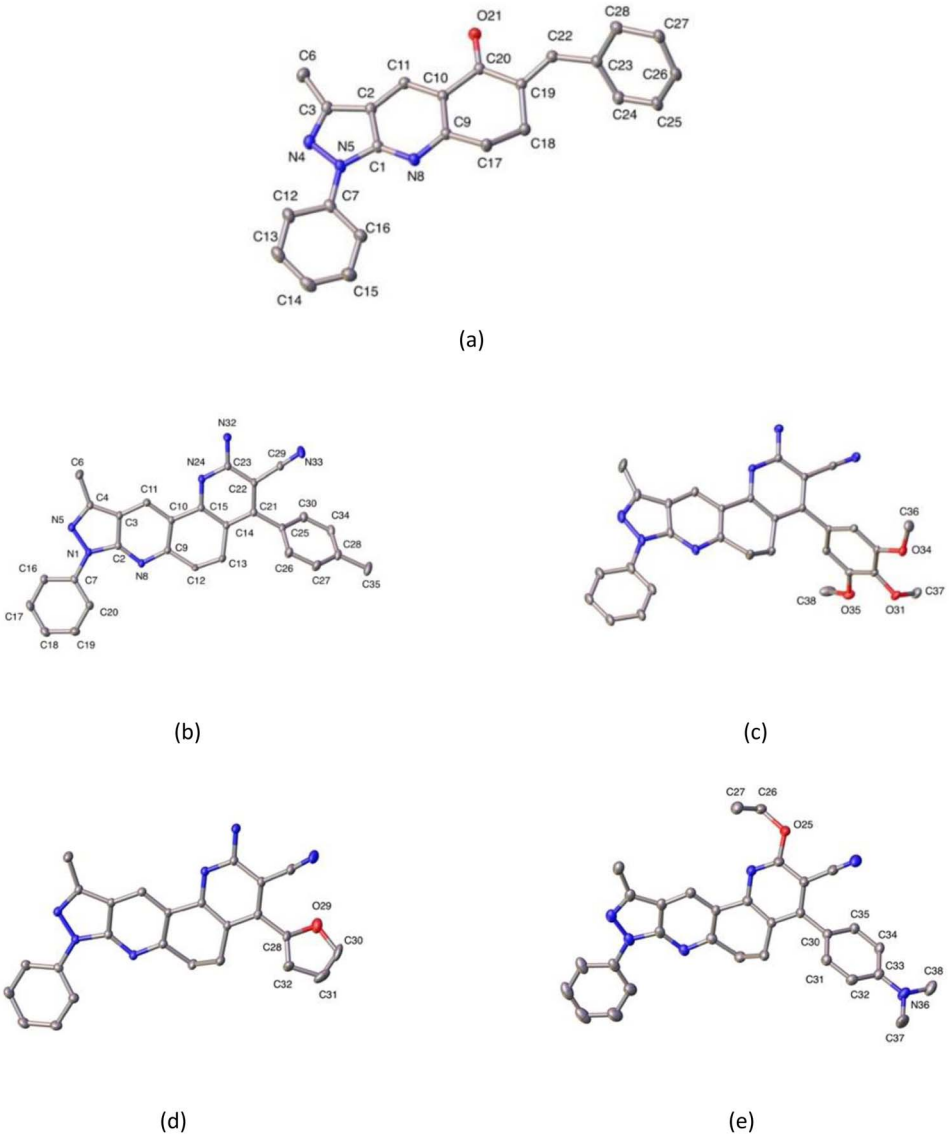

Fig. 5 ORTEP plots of compounds **3a** (a), **5b** (b) and, partially labeled **5j** (c), **5k** (d), and **5n** (e). Hydrogen atoms are omitted for the sake of clarity. Thermal ellipsoids were drawn with 30% of probability.

centrosymmetric rings with a graph-set notation $R_2 2(12)$, and $R_2 2(16)$, respectively.[58] In compound **3a**, the crystal packing is further stabilized by π–π stacking interaction between the pyridyl ring with a distance of 3.890 Å, angle of 6.309°, and slippage of 1.436 Å.

Table 4 Cremer and Pople parameters for compounds **3a**, **5b**, **5j**, **5k**, and **5n**

Compound	QT (Å)	θ (°)	φ (°)	Conformation
3a	0.380(3)	121.5(5)	85.4(4)	Screw-boat
5b	0.287(7)	90.0(2)	4.00(2)	Twist-boat
5j	0.418(3)	116.1(4)	93.4(4)	Screw-boat
5k	0.380(3)	61.7(5)	276.9(5)	Screw-boat
5n	0.467(4)	67.6(5)	274.1(6)	Screw-boat

2.5 Conformational analyses

Finally, all compounds show positional disorder over different fragments. In the case of compound **3a**, the phenyl ring was modeled over two positions with 0.5 occupancy ratio. In compound **5b**, the non-planar ring and nitrile fragment are disordered over three and two positions, respectively. These were modeled using a rigid model with 0.33 and 0.5 occupancy ratios on each part, respectively. In compound **5j** the phenyl ring is disordered over two positions. Modeling was done using FVAR in a 66 : 34 occupancy ratio, and in compound **5n**, the ethoxy fragment is disordered over two positions. Modeling was carried out using FVAR in a 70 : 30 occupancy ratio.

To determine which configuration of compounds **5b**, **5j**, **5k**, and **5n** is most stable, DFT energies were computed at different dihedral angle values between atoms 14, 21, 25, and 30 (compounds **5b**, **5j**, and **5k**) or 14, 21, 25, and 35 (compound **5n**)

Table 5 Intermolecular hydrogen bond interactions for compounds **3a**, **5b**, **5j**, and **5k**

Atoms	D–H (Å)	H···A (Å)	D···A (Å)	D–H···A (°)
3a				
C(17)–H(17B)···O(21)[a]	0.97	2.52	3.389	150.0
C(18)–H(18B)···O(21)[b]	0.97	2.58	3.407	143.0
5b				
N(32)–H(32A)··· N(33A)[c]	0.93	2.28	3.100	158.0
N(32)–H(32A)··· N(33B)[c]	0.88	2.28	3.10	159.0
N(32)–H(32B)···N(5)[d]	0.93	2.29	3.201	170.0
5j				
N(32)–H (32B)···N(33)[e]	0.87	2.49	3.167	136.0
5k				
N(32)–H (32A)···N(33)[f]	0.96	2.27	3.164	155.0
N(32)–H(32B)···N(5)[g]	0.94	2.40	3.310	165.0
C(32)–H(32)···N(32)[b]	0.93	2.55	3.410	154.0

[a] $x, 3/2 - y, -1/2 + z$. [b] $x, 3/2 - y, 1/2 + z$. [c] $1 - x, 1 - y, -z$. [d] $2 - x, 1/2 + y, 1/2 - z$. [e] $-x, 1 - y, 1 - z$. [f] $1 - x, 2 - y, 1 - z$. [g] $-x, 1/2 - y, 1/2 - z$.

(see Fig. 6). Table 6 and Fig. 7 show the conformation energies obtained for the analyzed compounds. These results reveal that for all compounds **5b**, **5j**, and **5n** in addition to the experimental angles determined by the crystallographic study other energy minima with nearly the same energy exist at angles around −90° and 120°. In addition, high rotational barriers of approximately 2.4 eV at angles of −180, 0, and 180° prevent the conversion between rotamers. On the other hand, for compound **5k** the experimental conformation is 0.07 eV more stable than the other possible rotamers, and it has a much lower rotational barrier of 0.14 eV at 0°. These observations are in qualitative agreement with the positional disorder observed in the X-ray analysis.

3. Experimental section

3.1 General information

The experiments were performed in Discover microwave apparatus (CEM Corporation, Matthews, NC, USA), while the ultrasonic irradiation was performed using a Branson Model 1510, 115v, 1.9 L Ultrasonic Bath with a mechanical timer (60 min with continuous hold), and a heater switch, 47 kHz. The ^{1}H and ^{13}C NMR spectra (400 MHz for proton and 100 MHz for carbon) were recorded on an AM-400 spectrometer (Bruker, Rheinstetten, Germany) using $CDCl_3$ and DMSO-d_6 as solvents. Tetramethylsilane (TMS) was used as an internal standard. IR spectra (KBr granules, 500–4000 cm^{-1}) were recorded on a NEXUS 670 FT-IR spectrophotometer (Thermo Nicolet, Madison, WI, USA). ESI-MS and ESI-MS/MS high-resolution mass spectrometry was carried out on a high resolution (Q) hybrid quadrupole time of flight (TOF) mass spectrometer (Waters/Micromass Q-TOF micro, Manchester, UK) with a constant nebulizer temperature of 100 °C. Melting points (uncorrected) were measured on an IA9100 electrothermal melting point device (Stone, Staffs, UK). The progress of the reaction was monitored by thin-layer chromatography (TLC) using silica gel 60 (Merck, Darmstadt, Germany). All reagents were purchased from Merck or Sigma Aldrich (St. Louis, MO, USA) and used without further purification. The final purification of all the products for the analysis was carried out by column chromatography, with the use of silica gel 60 (Merck 7734) with a particle size that fluctuates between 0.063 and 0.200 mm, with the eluent phase of ether mixtures of petroleum : ethyl acetate in increasing polarity.

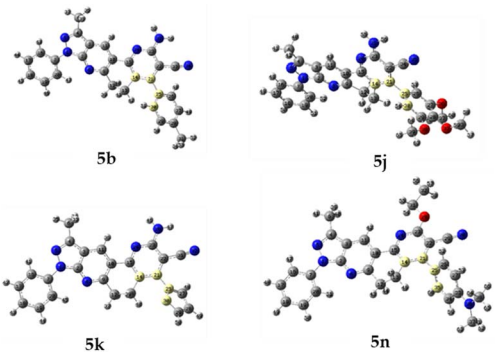

Fig. 6 Modified dihedral angle for molecules **5b**, **5j**, **5k**, and **5n**.

3.2 Chemistry

3.2.1 Synthesis by method A of 2-amino-10-methyl-4,8-diphenyl-6,8-dihydro-5*H*-pyrazolo[3,4-*j*][1,7]phenanthroline-3-carbonitrile (5a). A mixture of 3-methyl-1-phenyl-1,6,7,8-tetrahydro-5*H*-pyrazolo[3,4-*b*]quinolin-5-one (**2**, 1 mmol), benzaldehyde (**1a**, 1 mmol), KOH (1 lentil) and 3 mL of EtOH was placed in an ultrasonic bath for 5 minutes at room temperature. The resulting mixture was mixed with malononitrile (**4**, 1 mmol), 0.5 mL of AcOH, NH_4OAc (13 mmol), and 0.5 mL of

Table 6 Relative energies for hypothetical conformations, calculated for the products **5b**, **5j**, **5k** and **5n** at the B3LYP/6-31G* level of theory

	E relative (eV)			
Dihedral angle	**5b**	**5j**	**5k**	**5n**
−180	2.48	2.37	0.32	2.39
−120	0.01	0.20	0.07	0.01
−90	0.01	0.00	0.13	0.03
0	2.45	2.11	0.14	2.43
90	0.01	0.01	0.13	0.03
120	0.00	0.00	0.07	0.00
180	2.48	2.37	0.32	2.39
−59.1[a]	0.00	—	—	—
67.8	0.06	—	—	—
−57.6	—	0.12	—	—
71.3[a]	—	0.00	—	—
−47.5[a]	—	—	0.00	—
41	—	—	0.08	—
−59.6[a]	—	—	—	0.01
62.8	—	—	—	0.09

[a] Dihedral angle obtained in crystallographic analysis.

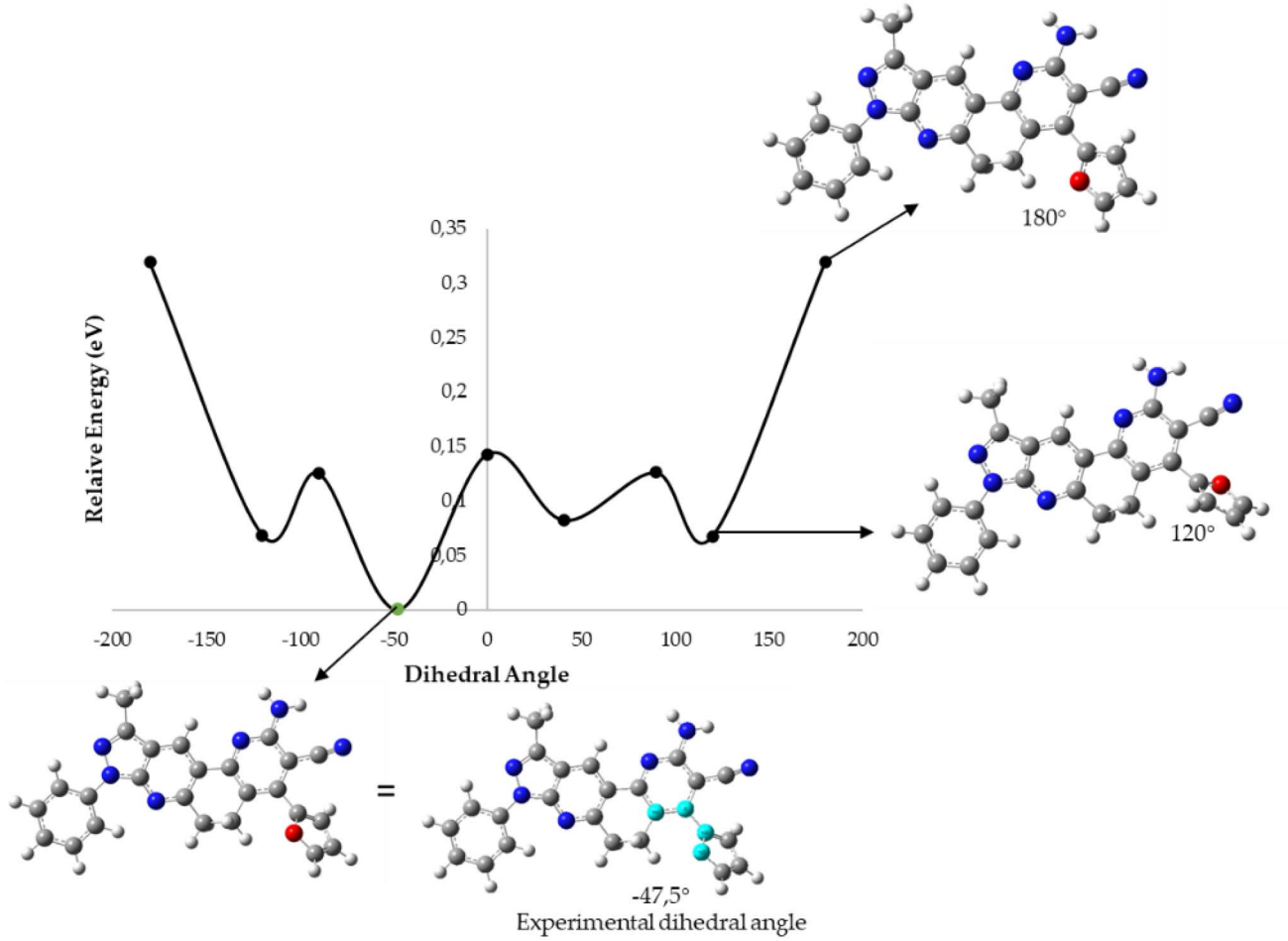

Fig. 7 B3LYP/6-31G* potential energy curve along the dihedral angle between the substituent ring and the fused DPH rings for the **5k** molecule.

dichloroethane (DCE) and subjected to MWI (at a maximum power of 200 W for 20 minutes at 120 °C). The reaction mixture was purified by using column chromatography with a petroleum ether/ethyl acetate mixture in increasing polarity as the eluent to give the corresponding derivative **5a**.

3.2.2 Synthesis by method B of 2-amino-10-methyl-8-phenyl-6,8-dihydro-5*H*-pyrazolo[3,4-*j*][1,7] phenanthroline-3-carbonitrile derivatives (5a–m). (a) A mixture of aromatic aldehyde (**1a–m**, 1 mmol), malononitrile (**4**, 1 mmol), proline (0.87 mmol), and 1 mL of EtOH was taken to an ultrasonic bath for 5 minutes at room temperature. (b) The resulting mixture was mixed with 3-methyl-1-phenyl-1,6,7,8-tetrahydro-5*H*-pyrazolo [3,4-*b*]quinolin-5-one (**2**, 1 mmol), 0.5 mL of AcOH, NH_4OAc (13 mmol), and 0.5 mL of DCE and was subjected to MWI (maximum power of 200 W for 20 minutes at 120 °C). The reaction mixture was purified by using column chromatography with a petroleum ether/ethyl acetate mixture in increasing polarity as the eluent to give the corresponding derivatives **5a–m**. The synthesized compounds with their physical data are listed below.

*3.2.2.1 2-Amino-10-methyl-4,8-diphenyl-6,8-dihydro-5H-pyrazolo[3,4-j][1,7]phenanthroline-3-carbonitrile **(5a)**.* Yield 59%; orange solid; mp 258–260 °C; IR (KBr, cm^{-1}): 3421, 3328, 3224, 2949, 2839, 2363, 2203, 1633, 1555, 1499, 1340, 1218, 1022, 747; ^1H NMR (400 MHz, DMSO-d_6); 2.60–2.64 (m, 5H), 3.03–3.07 (m, 2H), 6.86 (m, 2H), 7.28 (t, J = 8.0 Hz, 1H), 7.39 (dd, J = 8.0, 1.6 Hz, 2H), 7.50–7.56 (m, 6H), 8.26 (d, J = 8.0 Hz, 2H), 8.88 (s, 1H); ^{13}C NMR (400 MHz, DMSO-d_6); 12.2 (CH_3), 23.3 (CH_2), 31.5 (CH_2), 89.0 (C), 116.1 (C), 116.6 (C), 117.3(C), 119.9 (2 × CH), 123.6 (CH), 125.4 (CH), 127.3 (CH), 128.3 (2 × CH), 128.6 (C), 128.8 (CH), 129.0 (2 × CH), 129.1 (CH), 135.8 (C), 139.0 (C), 143.9 (C), 149.9 (C), 153.1 (C), 153.4 (C), 158.9 (C), 160.0 (C); HRMS (ESI, m/z): calcd for $C_{27}H_{21}N_6$ $[M + H]^+$ 429.1828 found 429.1830.

*3.2.2.2 2-Amino-10-methyl-8-phenyl-4-(p-tolyl)-6,8-dihydro-5H-pyrazolo[3,4-j][1,7]phenanthroline-3-carbonitrile **(5b)**.* Yield 47%; green solid; mp 218–220 °C; IR (KBr, cm^{-1}): 3494, 3473, 3354, 2952, 2214, 1612, 1601, 1546, 1502, 1375, 1245, 1111, 822; ^1H NMR (400 MHz, $CDCl_3$); 2.45 (s, 3H), 2.71 (s, 3H), 2.78–2.82 (m, 2H), 3.12–3.15 (m, 2H), 3.88 (s, 3H), 5.21 (s, 2H), 7.25–7.30 (m, 3H), 7.33–7.35 (m, 2H), 7.51 (t, J = 8.0 Hz, 2H), 8.30 (d, J = 8.0 Hz, 2H), 8.94 (s, 1H); HRMS (ESI, m/z): calcd for $C_{28}H_{23}N_6$ $[M + H]^+$ 443.1984 found 443.1989.

*3.2.2.3 2-Amino-4-(4-methoxyphenyl)-10-methyl-8-phenyl-6,8-dihydro-5H-pyrazolo[3,4-j][1,7]phenanthr-oline-3-carbonitrile **(5c)**.* Yield 50%; yellow solid; mp 253–255 °C; IR (KBr, cm^{-1}): 3485,

3355, 2949, 2212, 1598, 1508, 1245, 1178, 1028; ^{1}H NMR (400 MHz, $CDCl_3$); 2.70 (s, 3H), 2.79–2.83 (m, 2H), 3.11–3.15 (m, 2H), 3.88 (s, 3H), 5.19 (s, 2H), 7.03–7.06 (m, 3H), 7.27–732 (m, 2H), 7.50 (t, J = 8.0 Hz, 2H), 8.30 (d, J = 8.0 Hz, 2H), 8.91 (s, 1H); HRMS (ESI, m/z): calcd for $C_{28}H_{23}N_6O$ $[M + H]^+$ 459.1933 found 459.1930.

3.2.2.4 2-Amino-4-(4-chlorophenyl)-10-methyl-8-phenyl-6,8-dihydro-5H-pyrazolo[3,4-j][1,7]phenanthroline-3-carbonitrile ***(5d).*** Yield 46%; orange solid; mp 282–284 °C; IR (KBr, cm^{-1}): 3467, 3349, 3236, 2961, 2214, 1630, 1598, 1497, 1433, 1245, 1328, 1082, 753; ^{1}HNMR (400 MHz, DMSO-d_6); 2.61–2.65 (m, 5H), 3.06–3.09 (m, 2H), 6.91 (m, 2H), 7.30 (t, J = 7.5 Hz, 1H), 7.46 (d, J = 8.6 Hz, 2H), 7.52–7.56 (m, 2H), 7.61–763 (m, 2H), 8.27 (d, J = 8.8 Hz, 2H), 8.91 (s, 1H); HRMS (ESI, m/z): calcd for $C_{27}H_{20}ClN_6$ $[M + H]^+$ 463.1438 found 463.1441.

3.2.2.5 2-Amino-10-methyl-4-(4-nitrophenyl)-8-phenyl-6,8-dihydro-5H-pyrazolo[3,4-j][1,7]phenanthroline-3-carbonitrile ***(5e).*** Yield 46%; orange solid; mp 282–284 °C; IR (KBr, cm^{-1}): 3467, 3349, 3236, 2961, 2214, 1630, 1598, 1497, 1433, 1245, 1328, 1082, 753; ^{1}HNMR (400 MHz, DMSO-d_6); 2.45–2.46 (m, 2H), 2.65 (m, 3H), 2.97–2.98 (m, 2H), 6.70 (m, 2H), 7.31 (t, J = 7.0 Hz, 1H), 7.44–7.46 (m, 2H), 7.53–7.57 (m, 2H), 7.63 (d, J = 8.3 Hz, 2H), 8.26 (d, J = 8.6 Hz, 2H), 9.01 (s, 1H); HRMS (ESI, m/z): calcd for $C_{27}H_{20}N_7O_2$ $[M + H]^+$ 474.1678 found 474.1683.

3.2.2.6 2-Amino-4-(2-chloroquinolin-3-yl)-10-methyl-8-phenyl-6,8-dihydro-5H-pyrazolo[3,4-j][1,7]phenanthroline-3-carbonitrile ***(5f).*** Yield 30%; yellow solid; mp 295–297 °C; IR (KBr, cm^{-1}): 3410, 3320, 3050,2960, 2900, 2200, 1560, 1500, 1410, 1330, 1140, 1030, 756; ^{1}HNMR (400 MHz, DMSO-d_6); 2.60 (t, J = 7.3 Hz, 2H), 2.64 (s, 3H), 3.09–3.12 (m, 2H), 7.11 (s, 2H), 7.03–7.06 (m, 3H), 7.29 (t, J = 7.3 Hz, 1H), 7.51–7.56 (m, 2H), 7.77 (t, J = 7.5 Hz, 1H), 7.93–7.97 (m, 1H), 8.08–8.15 (m, 2H), 8.26 (t, J = 9.3 Hz, 2H), 8.67 (s, 1H), 8.95 (s, 1H); HRMS (ESI, m/z): calcd for $C_{30}H_{21}ClN_7$ $[M + H]^+$ 514.1547 found 514.1548.

3.2.2.7 2-Amino-4-(4-hydroxyphenyl)-10-methyl-8-phenyl-6,8-dihydro-5H-pyrazolo[3,4-j][1,7]phenanthroline-3-carbonitrile ***(5g).*** Yield 28%; red solid; mp > 300 °C; IR (KBr, cm^{-1}): 3390, 3336, 3217, 3064,2937, 2870, 2204, 1583, 1510, 1441, 1176, 758; NMR (400 MHz, DMSO-d_6); 2.15–2.17 (m, 2H), 2.60 (s, 3H), 2.89–3.00 (m, 2H), 6.78 (d, J = 8.8 Hz, 2H), 7.23–7.29 (m, 4H), 7.53 (t, J = 7.1 Hz, 2H), 7.66 (bs, 2H), 8.26 (d, J = 7.6 Hz, 2H), 8.31 (s, 1H), 9.72 (s, 1H); HRMS (ESI, m/z): calcd for $C_{27}H_{23}N_6O$ $[M + 3H]^+$ 447.1933 found 447.2064.

3.2.2.8 2-Amino-4-(4-cyanophenyl)-10-methyl-8-phenyl-6,8-dihydro-5H-pyrazolo[3,4-j][1,7]phenanthroline-3-carbonitrile ***(5h).*** Yield 33%; yellow solid; mp > 300 °C; IR (KBr, cm^{-1}): 3426, 3355, 3056, 2927, 2208, 1590, 1546, 1411, 1334, 1251, 904, 746; ^{1}H NMR (400 MHz, DMSO-d_6); 2.60–2.64 (m, 5H), 3.06–3.10 (m, 2H), 6.98 (m, 2H), 7.30 (t, J = 6.7 Hz, 1H), 7.53 (t, J = 7.9 Hz, 2H), 7.65 (t, J = 7.6 Hz,H), 8.04 (d, J = 8.3 Hz, 2H), 8.26 (t, J = 8.8 Hz, 2H), 8.92 (s, 1H); HRMS (ESI, m/z): calcd for $C_{28}H_{20}N_7$ $[M + H]^+$ 454.1780 found 454.1808.

3.2.2.9 2-Amino-10-methyl-8-phenyl-4-(pyridin-3-yl)-6,8-dihydro-5H-pyrazolo[3,4-j][1,7]phenanthroline-3-carbonitrile ***(5i).*** Yield 41%; yellow solid; mp 245–247 °C; ^{1}H NMR (400 MHz, $CDCl_3$); 2.70 (s, 3H), 2.99–3.04 (m, 2H), 3.11–3.15 (m, 2H), 5.26 (s, 2H), 7.27–7.32 (m, 1H), 7.48–7.52 (m, 3H), 7.72–7.76 (m, 1H), 8.28 (t, J = 8.9 Hz, 2H), 8.62 (dd, J = 1.5, 12.5 Hz, 1H), 8.76 (d, J = 4.9 Hz, 1H), 8.93 (s, 1H); HRMS (ESI, m/z): calcd for $C_{26}H_{20}N_7$ $[M + H]^+$ 430.1780 found 430.1781.

3.2.2.10 2-Amino-10-methyl-8-phenyl-4-(3,4,5-trimethoxyphenyl)-6,8-dihydro-5H-pyrazolo[3,4-j][1,7]phenanthroline-3-carbonitrile ***(5j).*** Yield 49%; yellow solid; mp 273–275 °C; IR (KBr, cm^{-1}): 3460, 3348, 3055, 2936,2833, 2212, 1589, 1417, 1240, 1125, 1001, 758; ^{1}H NMR ($CDCl_3$, 400 MHz): 2.60 (s, 3H), 3.20 (s, 4H), 3.83 (s, 9H), 6.64 (s, 2H), 7.20–7.25 (m, 2H), 7.44 (t, J = 7.5 Hz, 2H), 7.81 (m, 1H), 8.23 (d, J = 7.8 Hz, 2H), 8.74 (s, 1H); HRMS (ESI, m/z): calcd for $C_{30}H_{26}N_6O_3$ $[M + H]^+$ 519.2145 found 519.2164.

3.2.2.11 2-Amino-4-(furan-2-yl)-10-methyl-8-phenyl-6,8-dihydro-5H-pyrazolo[3,4-j][1,7]phenanthroline-3-carbonitrile ***(5k).*** Yield 33%; red crystal; mp 219–221 °C; IR (KBr, cm^{-1}): ^{1}H NMR (400 MHz, $CDCl_3$); 2.67 (s, 3H), 3.31 (t, J = 6.4 Hz, 2H) 3.40 (t, J = 6.2 Hz, 2H), MHz, $CDCl_3$); 2.67 (s, 3H), 3.31 (t, J = 6.4 Hz, 2H) 3.40 (t, J = 6.2 Hz, 2H), 6.54 (s, 1H), 6.75–6.76 (m, 1H), 7.26–7.31 (m, 2H), 7.51 (t, J = 7.5 Hz, 2H), 7.60 (s, 1H), 7.65 (s, 1H), 8.29 (d, J = 8.3 Hz, 2H), 8.79 (s, 1H); HRMS (ESI, m/z): calcd for $C_{25}H_{18}N_6NaO$ $[M + Na]^+$ 441.1440 found 441.1260.

3.2.2.12 2-Amino-4-(benzo[d][1,3]dioxol-5-yl)-10-methyl-8-phenyl-6,8-dihydro-5H-pyrazolo[3,4-j][1,7]phenanthroline-3-carbonitrile ***(5l).*** Yield 7%; yellow solid; mp > 300 °C; IR (KBr, cm^{-1}): 3431, 3336, 3221,3053, 2937, 2854, 2210, 1720, 1593, 1493, 1355, 1248, 1093, 1038, 926, 818; ^{1}H NMR (400 MHz, $CDCl_3$); 2.71 (s, 3H), 3.29 (bs, 2H), 6.06 (s, 2H), 6.92 (d, J = 7.8 Hz, 1H), 7.02–7.06 (m, 2H), 7.31–7.35 (m, 1H), 7.54 (t, J = 7.6 Hz, 2H), 7.90 (s, 1H), 8.32 (t, J = 8.1 Hz, 2H), 8.85 (s, 1H); HRMS (ESI, m/z): calcd for $C_{28}H_{20}N_6NaO_2$ $[M + Na]^+$ 495.1545 found 495.1547.

*3.2.2.13 2-Amino-10-methyl-8-phenyl-4-(quinolin-3-yl)-6,8-dihydro-5H-pyrazolo[3,4-j][1,7]phenanthroline-3-carbonitrile (****5m****).* Yield 38%; orange solid; mp 258–260 °C; IR (KBr, cm^{-1}): 3419, 3062, 2958 2927, 2202, 1599, 1462, 1277, 1122, 1072, 744; ^{1}H NMR (400 MHz, DMSO-d_6); 2.65 (s, 3H), 2.69–2.75 (m, 2H), 3.08–3.13 (m, 2H), 7.01 (s, 2H), 7.29 (t, J = 7.5 Hz, 1H), 7.52–7.55 (m, 2H), 7.73 (t, J = 7.6 Hz, 1H), 7.87–7.91 (m, 1H), 8.12 (dd, J = 8.1, 12.9 Hz, 2H), 8.28 (d, J = 7.6 Hz, 2H), 8.54 (s, 1H), 8.9–8.96 (m, 2H); HRMS (ESI, m/z): calcd for $C_{30}H_{21}N_7$ $[M]^+$ 479.1858 found 479.2041; calcd for $C_{30}H_{20}N_7$ $[M - H]^+$ 478.1780 found 478.2022.

3.2.3 *Synthesis by method C of 2-ethoxy-10-methyl-4,8-diphenyl-6,8-dihydro-5H-pyrazolo[3,4-j][1,7] phenanthroline-3-carbonitrile derivatives (5n–p).* A mixture of aromatic aldehyde (**1n–p**, 1 mmol), malononitrile (**4**, 1 mmol), proline (0.87 mmol), and 1 mL of EtOH was taken to an ultrasonic bath for 5 minutes at room temperature. The resulting mixture was mixed with 3-methyl-1-phenyl-1,6,7,8-tetrahydro-5*H*-pyrazolo[3,4-*b*] quinolin-5-one (**2**, 1 mmol), NaH (4 mmol) and 5 mL of ethanol. Then, the reaction mixture was refluxed for 3 h at 80 ° C. The reaction was monitored by TLC. After completion of the reaction, the reaction mixture was poured into ice water and neutralized with HCl (10 mL, 2 N). The precipitate was filtered and washed with water. The product was purified through column chromatography with EtOAc/petroleum ether gradient (3 : 7) as the eluent, resulting in compounds **5n–p**.

*3.2.3.1 4-(4-(Dimethylamino)phenyl)-2-ethoxy-10-methyl-8-phenyl-6,8-dihydro-5H-pyrazolo[3,4-j][1,7]phenanthroline-3-carbonitrile (**5n**).* Yield 42%; orange crystal; mp > 300 °C IR (KBr, cm^{-1}): 3039, 2970, 2870, 2212, 1649, 1556, 1254, 1349, 1107, 835; ^{1}H NMR (400 MHz, $CDCl_3$); 1.56 (t, J = 7.1 Hz, 3H), 2.72 (s, 3H), 3.04 (s, 3H), 3.12–3.14 (m, 2H), 3.36–3.38 (m, 2H), 4.69 (q, J = 7.1 Hz, 2H), 6.81 (d, J = 8.8 Hz, 2H), 7.24–7.26 (t, J = 8.0 Hz, 3H), 7.43 (m, 2H), 8.26 (d, J = 8.0 Hz, 2H), 8.8.84 (s, 1H).

*3.2.3.2 2-Ethoxy-4-(4-methoxyphenyl)-10-methyl-8-phenyl-6,8-dihydro-5H-pyrazolo[3,4-j][1,7]phenanthroline-3-carbonitrile (**5o**).* Yield 61%; yellow solid; mp > 300 °C; ^{1}H NMR (400 MHz, $CDCl_3$); 1.52 (t, J = 7.0 Hz, 3H), 2.65 (s, 3H), 2.79 (t, J = 7.2 Hz, 2H), 3.08 (t, J = 7.2 Hz, 2H), 3.83 (s, 3H), 4.63 (q, J = 7.0 Hz, 2H), 7.00 (d, J = 8.0 Hz, 2H), 7.23 (t, J = 8.0 Hz, 3H), 7.43 (t, J = 8.0 Hz, 2H), 8.26 (d, J = 8.0 Hz, 2H), 8.72 (s, 1H); ^{13}C NMR (100 MHz, $CDCl_3$); 12.5 (CH_3), 14.4 (CH_3), 24.1 (CH_2), 31.8 (CH_2), 55.2 (CH_3), 63.0 (CH_2), 95.1 (C), 114.1 (2 × CH), 115.5 (C), 116.6 (C), 120.4 (2 × CH), 121.9 (C), 123.6 (C), 125.4 (CH), 127.0 (C), 127.1 (CH), 128.8 (2 × CH), 129.9 (2 × CH), 139.3 (C), 143.8 (C), 150.4 (C), 152.5 (C), 155.2 (C), 159.4 (C), 160.2 (C), 162.9 (C); HRMS (ESI, m/z): calcd for $C_{30}H_{25}N_5O_2$ $[M]^+$ 487.2008 found 487.2138.

*3.2.3.3 2-Ethoxy-10-methyl-4,8-diphenyl-6,8-dihydro-5H-pyrazolo[3,4-j][1,7]phenanthroline-3-carbonitrile (**5p**).* Yield 52%; yellow solid; mp > 300 °C; IR (KBr, cm^{-1}): 3049, 2968, 2864, 2218, 1606, 1506, 1381, 1254, 1146, 1024, 822, 754; ^{1}H NMR (400 MHz, $CDCl_3$); 1.44 (t, J = 7.0 Hz, 3H), 2.59 (s, 3H), 2.69 (t, J = 7.2 Hz, 2H), 3.01 (t, J = 7.2 Hz, 2H), 4.57 (q, J = 7.0 Hz, 2H), 7.14 (t, J = 8.0 Hz, 1H), 7.22 (d, J = 8.0 Hz, 2H), 7.35–7.41 (m, 5H), 8.17 (d, J = 8.0 Hz, 2H), 8.70 (s, 1H); ^{13}C NMR (100 MHz, $CDCl_3$); 12.5 (CH_3), 14.5 (CH_3), 24.1 (CH_2), 31.8(CH_2), 63.1 (CH_2), 95.1 (C), 115.3 (C), 116.7 (C), 120.6 (2 × CH), 121.8 (C), 123.6 (C), 125.6 (CH), 127.3 (CH), 128.3 (2 × CH), 128.8 (2 × CH), 128.9 (2 × CH), 129.2 (CH), 135.1 (C), 139.3 (C), 143.9 (C), 150.5 (C), 152.8 (C), 155.4 (C), 159.6 (C), 162.9 (C); HRMS (ESI, m/z): calcd for $C_{29}H_{24}N_5O$ $[M + H]^+$ 458.1981 found 458.2120.

3.3 Biological activity

3.3.1 Anticholinesterase assay. The enzymatic inhibition turned into finished through making use of the spectrophotometric technique of Ellman AChE (from *Electrophorus electricus*) and BChE (from equine serum),[59] 5,5′-dithio-bis-(2-nitrobenzoic acid) (DTNB), acetylthiocholine and butyrylthiocholine iodides, were purchased from Sigma-Aldrich. Stock solutions of test compounds were made up in 100 μL of DMSO and 900 μL of phosphate buffer (8 mmol L^{-1} K_2HPO_4, 2.3 mmol L^{-1} NaH_2PO_4, 150 mmol L^{-1} NaCl and Tween 20 at 0.05% at pH 7.6). In a 96–well plate, 50 μL of stock solutions were diluted with phosphate buffer to obtain concentrations between 15 and 500 μg mL^{-1} for each compound (**5a–p**). Enzyme solutions with buffer were prepared to give 0.25 units per mL, and 50 μL was added to the plate. After 30 minutes of incubation, the substrate solution consisting of Na_2HPO_4 (40 mmol L^{-1}), acetylthiocholine/butyrylthiocholine (0.24 mmol L^{-1}), and DTNB (0.2 mmol L^{-1}) was added, the mixture was incubated for another 5 minutes and absorption at 405 nm was determined with a microtiter plate reader (Multiskan EX, Thermo). Each compound concentration was tested in triplicate. IC_{50} values were calculated by regression analysis.

3.3.2 Measurement of DPPH radical scavenging activity. The newly synthesized compounds **5a–p** were evaluated for $DPPH^{\bullet+}$ free radical scavenging activity. According to the method previously described and adapted,[60] a 1 mL aliquot of the tested compound (10–100 μg mL^{-1}) and the control (2% final DMSO) were taken, respectively, and mixed with 2 mL of a methanolic $DPPH^{\bullet+}$solution (0.02 mg mL^{-1}). The mixture was vigorously stirred and left to stand at room temperature for 5 minutes in the absence of light; after this time, the sample was taken to a spectrophotometer at 517 nm to determine its absorbance. Free radical scavenging activity was calculated as a percentage of $DPPH^{\bullet+}$ discoloration using the following equation:

$$\text{Percentage of free radical removal } DPPH^{\bullet+} = 100 \times (1 - AE/AD) \quad (1)$$

where AE is the absorbance of the solution after adding the sample, and AD is the absorbance of the blank DPPH solution. Ascorbic acid was used as the reference compound with an EC_{50} value of 1.5 μg mL^{-1}.

3.3.3 Measurement of ABTS radical scavenging activity. The newly synthesized compounds **5a–p** were evaluated for the radical scavenging activity of $ABTS^{\bullet+}$ according to a published test.[61] The stock solution was prepared by mixing equal volumes of a solution of 7 mM ABTS and a 2.45 mM potassium persulfate solution followed by incubation for 12 h at room temperature in the dark to produce a dark-colored solution containing $ABTS^{\bullet+}$ radicals. The working solution was prepared once it was needed in the assay to avoid its oxidation, adding 50% ethanol to give an initial absorbance of approximately 0.700 (+0.02) at 732 nm at room temperature. Free radical scavenging activity was evaluated by mixing 300 μL of different compounds (10–200 μg mL^{-1} in the respective solvents) with 3.0 mL of $ABTS^{\bullet+}$ working standard. The decrease in absorbance was measured exactly 1 minute after mixing the solution; the final absorbance was observed after 6 min. Ascorbic acid, with an EC_{50} value of 28 μg mL^{-1}, was used as a positive control. The elimination activity was estimated based on the percentage of $ABTS^{\bullet+}$ radicals eliminated using the following equation:

$$\text{Percentage of free radical removal } ABTS^{\bullet+} = [(A_0 - A_s)/A_0] \times 100 \quad (2)$$

where A_0 is the absorption of the control, and A_s is the absorption of the test compound solution.

3.4 X-Ray diffraction measurements

Crystals of compounds **3a**, **5b**, **5j**, **5k** and **5n** were measured and their diffraction data were collected at *ca.* 296 K with a D8 Venture diffractometer equipped with a bidimensional CMOS Photon 100 detector, using graphite monochromated Mo-Kα (λ = 0.71073 Å). The diffraction frames were integrated using the APEX3 package[62] and were corrected for absorptions with

SADABS. The structure of the title compound was solved by intrinsic phasing[63] using the OLEX 2 program.[64] All the structures were then refined with the full-matrix least-squares method based on F^2 (SHELXL-2014).[63] X-ray crystal structure determinations, CIF files containing tables of crystallographic parameters, bond lengths, bond angles, and a list of structure factors have been deposited in the Cambridge Crystallographic Data Centre (CCDC no. 2200163–2200166 and 2203148).

3.5 Computational methods

Density functional theory (DFT) was employed to optimize the ground state geometries and to compute the vibrational frequencies of the **5a–5p** molecules. These calculations were performed with the Gaussian 16 computational package using the B3LYP functional and the 6-31G* basis set.[65–70] The calculated vibrational frequencies were scaled by 0.9627.

The ionization potential (IP) and the electronic affinity (EA) were estimated from the highest occupied molecular orbital (HOMO) and the lowest unoccupied molecular orbital (LUMO) energies as IP = −εHOMO and as EA = −εLUMO. These estimates were employed to compute the electronegativity (χ), chemical hardness (η) and softness (S) parameters as $\chi = (\mathrm{IP} + \mathrm{EA})/2$, $\eta = (\mathrm{IP} - \mathrm{EA})/2$ and $S = 1/\eta$.[53]

Molecular docking was performed using Glide[71] (Schrödinger Release 2021-2: 2021d. Glide. Schrödinger, LLC New York, NY.) software within the Schrödinger Small-Molecule Drug Discovery Suite. The atomic coordinates for human AChE protein were extracted from the Protein Data Base (PDB ID: 4EY7). LigPrep (Schrödinger Release 2021-2: 2021c. LigPrep. Schrödinger, LLC New York, NY.) and Preparation Wizard (Schrödinger Release 2021-2:, 2021b. Protein Preparation Wizard. Epik, Schrödinger, LLC, New York, NY.) module were used to obtain the minimized energy structure of the ligand and optimize the AChE enzyme, respectively, under the OPLS-AA force field.[72] The absorption, distribution, metabolism, and excretion properties of the compounds were predicted using SwissADME (**https://www.swissadme.ch**) open access software.

4. Conclusions

In conclusion, a total of 16 new pyrazol[3,4-*j*][1,7] phenanthroline-3-carbonitrile derivatives were synthesized, with amino (**5a–m**) and ethoxy (**5n–p**) groups in position 2. Two synthetic methodologies were used to obtain derivatives **5a–m**, where method B presented better results with respect to reaction times, yields and easy workability. Likewise, a third methodology was used to efficiently obtain the **5n–p** compounds.

The synthesized compounds were evaluated for their antioxidant activity with the aid of DPPH and ABTS assays. Compound **5e** stood out for having the best results of DPPH assay, presenting an EC_{50} value of 25 μg mL^{-1}. Additionally, in the ABTS test, compounds **5e**, **5f**, and **5g** presented the best results with EC_{50} values of 11.51, 3.1 and <3 μg mL^{-1}, evidencing even better results than the ascorbic acid that was used as a positive control. Structure-antioxidant activity relationship studies indicate that compound **5e** has a strong ability to accept electrons, supporting a radical state, and it can also react with soft species such as DPPH and ABTS radicals. Additionally, the compounds showed moderate activity as cholinergic inhibitors, with compounds **5c** and **5l** being the most active on AChE and BChE, respectively. In addition, the pharmacokinetic and pharmacodynamic properties analyzed *in silico* demonstrate that the new molecular entities are as oral drugs promising to be used. Finally, DFT studies reasonably predicted the conformations with lower relative energy of the crystallized compounds **5b**, **5j**, **5k**, and **5n**.

Author contributions

Efraín Polo-Cuadrado: investigation, methodology, and writing – original draft; Cristian Rojas-Peña: investigation, methodology, and writing – original draft; Karen Acosta-Quiroga: investigation, methodology, and writing – original draft; Lorena Camargo-Ayala: investigation, methodology, and writing – original draft; Iván Brito: writing – original draft, visualization, and software; Jonathan Cisterna: writing – original draft, visualization, and software; Félix Moncada: data curation, software, visualization, conceptualization, and writing – original draft; Jorge Trilleras: writing – review & editing and supervision; Yeray A. Rodríguez-Núñez: conceptualization, methodology, and writing – original draft; Margarita Gutiérrez: project administration, resources, supervision, and writing – review & editing.

Conflicts of interest

There are no conflicts to declare.

Acknowledgements

The authors acknowledge the Research Group of the Laboratory of Organic Synthesis and Biological Activity of the University of Talca. E. P-C. thanks FONDECYT Post-Doctoral Fellowship No. 3220681. Fondecyt Project 1200531 and the ANID National Doctorate Scholarship 2019 Folio No. 21190020. The authors also acknowledge FONDEQUIP program (EQM 130021, 160063 and 180024).

Notes and references

1 T. Shiro, T. Fukaya and M. Tobe, *Eur. J. Med. Chem.*, 2015, **97**, 397–408.
2 F. Salehian, H. Nadri, L. Jalili-Baleh, L. Youseftabar-Miri, S. N. Abbas Bukhari, A. Foroumadi, T. Tüylü Küçükkilinç, M. Sharifzadeh and M. Khoobi, *Eur. J. Med. Chem.*, 2021, **212**, 113034.
3 M. S. Salem and M. A. M. Ali, *Biol. Pharm. Bull.*, 2016, **39**, 473–483.
4 L. W. Mohamed, M. A. Shaaban, A. F. Zaher, S. M. Alhamaky and A. M. Elsahar, *Bioorg. Chem.*, 2019, **83**, 47–54.
5 R. Lin, P. J. Connolly, Y. Lu, G. Chiu, S. Li, Y. Yu, S. Huang, X. Li, S. L. Emanuel, S. A. Middleton, R. H. Gruninger, M. Adams, A. R. Fuentes-Pesquera and L. M. Greenberger, *Bioorg. Med. Chem. Lett.*, 2007, **17**, 4297–4302.

6 M. A. El-borai, H. F. Rizk, M. F. Abd-Aal and I. Y. El-Deeb, *Eur. J. Med. Chem.*, 2012, **48**, 92–96.
7 T. El-Sayed Ali, *Eur. J. Med. Chem.*, 2009, **44**, 4385–4392.
8 M. S. Nafie, A. M. Amer, A. K. Mohamed and E. S. Tantawy, *Bioorg. Med. Chem.*, 2020, **28**, 115828.
9 R. Aggarwal, S. Kumar, R. Sadana, A. Guzman and V. Kumar, *Synth. Commun.*, 2021, **51**, 3308–3324.
10 D. M. Volochnyuk, S. V. Ryabukhin, A. S. Plaskon, Y. V. Dmytriv, O. O. Grygorenko, P. K. Mykhailiuk, D. G. Krotko, A. Pushechnikov and A. A. Tolmachev, *J. Comb. Chem.*, 2010, **12**, 510–517.
11 S. A. Ibrahim, H. F. Rizk, M. A. El-Borai and M. E. Sadek, *J. Iran. Chem. Soc.*, 2021, **18**, 1391–1404.
12 G. Pandey, S. Bhowmik and S. Batra, *Org. Lett.*, 2013, **15**, 5044–5047.
13 B. Orlikova, W. Chaouni, M. Schumacher, M. Aadil, M. Diederich and G. Kirsch, *Eur. J. Med. Chem.*, 2014, **85**, 450–457.
14 H. Saggadi, D. Luart, N. Thiebault, I. Polaert, L. Estel and C. Len, *RSC Adv.*, 2014, **4**, 21456–21464.
15 S. M. H. Sanad and A. E. M. Mekky, *Chem. Biodivers.*, 2021, **19**, e202100500.
16 M. McCann, A. Kellett, K. Kavanagh, M. Devereux and A. L. S. Santos, *Curr. Med. Chem.*, 2012, **19**, 2703–2714.
17 N. L. Stevanović, T. P. Andrejević, A. Crochet, T. Ilic-Tomic, N. S. Drašković, J. Nikodinovic-Runic, K. M. Fromm, M. I. Djuran and B. Đ. Glišić, *Polyhedron*, 2019, **173**, 114112.
18 N. D. Savić, S. Vojnovic, B. Glišić, A. Crochet, A. Pavic, G. V. Janjić, M. Pekmezović, I. M. Opsenica, K. M. Fromm, J. Nikodinovic-Runic and M. I. Djuran, *Eur. J. Med. Chem.*, 2018, **156**, 760–773.
19 M. A. Smith, K. Hirai, K. Hsiao, M. A. Pappolla, P. L. R. Harris, S. L. Siedlak, M. Tabaton and G. Perry, *J. Neurochem.*, 1998, **70**, 2212–2215.
20 E. H. Edinsha Gladis, K. Nagashri and J. Joseph, *Inorg. Chem. Commun.*, 2020, **122**, 108232.
21 L. Tabrizi, D. Q. Dao and T. A. Vu, *RSC Adv.*, 2019, **9**, 3320–3335.
22 H. Mutlu Gençkal, *J. Mol. Struct.*, 2020, **1209**, 127917.
23 T. Pan, S. Xie, Y. Zhou, J. Hu, H. Luo, X. Li and L. Huang, *Bioorg. Med. Chem. Lett.*, 2019, **29**, 2150–2152.
24 T. Umar, S. Shalini, M. K. Raza, S. Gusain, J. Kumar, P. Seth, M. Tiwari and N. Hoda, *Eur. J. Med. Chem.*, 2019, **175**, 2–19.
25 C. Bancher, C. Brunner, H. Lassmann, H. Budka, K. Jellinger, G. Wiche, F. Seitelberger, I. Grundke-Iqbal, K. Iqbal and H. M. Wisniewski, *Brain Res.*, 1989, **477**, 90–99.
26 M. P. Murphy and H. Levine, *J. Alzheimer's Dis.*, 2010, **19**, 311–323.
27 D. S. Eisenberg and M. R. Sawaya, *Nature*, 2017, **547**, 170–171.
28 M. G. Savelieff, S. Lee, Y. Liu and M. H. Lim, *ACS Chem. Biol.*, 2013, **8**, 856–865.
29 K. P. Kepp, *Prog. Neurobiol.*, 2016, **143**, 36–60.
30 A. C. Andorn and R. N. Kalaria, *J. Alzheimer's Dis.*, 2000, **2**, 69–78.
31 M. Rosini, E. Simoni, A. Milelli, A. Minarini and C. Melchiorre, *J. Med. Chem.*, 2014, **57**, 2821–2831.
32 J. Apelt, M. Bigl, P. Wunderlich and R. Schliebs, *Int. J. Dev. Neurosci.*, 2004, **22**, 475–484.
33 F. Collin, C. Cheignon and C. Hureau, *Biomarkers Med.*, 2018, **12**, 201–203.
34 J. M. Carney, P. E. Starke-Reed, C. N. Oliver, R. W. Landum, M. S. Cheng, J. F. Wu and K. A. Floyd, *Proc. Natl. Acad. Sci. U. S. A.*, 1991, **88**, 3633–3636.
35 A. Kontush, *Free Radical Biol. Med.*, 2001, **31**, 1120–1131.
36 C. Cheignon, M. Tomas, D. Bonnefont-Rousselot, P. Faller, C. Hureau and F. Collin, *Redox Biol.*, 2018, **14**, 450–464.
37 E. Polo, K. Ferrer-Pertuz, J. Trilleras, J. Quiroga and M. Gutiérrez, *RSC Adv.*, 2017, **7**, 50044–50055.
38 J. Wang, Z. Li, X. Wang, Y. Zhou and C. Guo, *Heterocycles*, 2015, **91**, 49–63.
39 M. Venkatanarayana and P. K. Dubey, *Synth. Commun.*, 2012, **42**, 1746–1759.
40 R. Chatterjee, S. Bhukta and R. Dandela, *J. Heterocycl. Chem.*, 2022, **59**, 633–654.
41 S. M. Roopan, A. Bharathi, J. Palaniraja, K. Anand and R. M. Gengan, *RSC Adv.*, 2015, **5**, 38640–38645.
42 M. Karabacak, M. Çinar and M. Kurt, *J. Mol. Struct.*, 2008, **1–3**, 28–35.
43 D. C. Christodouleas, C. Fotakis, A. Nikokavoura, K. Papadopoulos and A. C. Calokerinos, *Food Anal. Methods*, 2015, **8**, 1294–1302.
44 M. P. Rigobello, R. Stevanato, F. Momo, S. Fabris, G. Scutari, R. Boscolo, A. Folda and A. Bindoli, *Free Radical Res.*, 2004, **38**, 315–321.
45 W. B. Li, X. P. Qiao, Z. X. Wang, S. Wang and S. W. Chen, *Bioorg. Chem.*, 2020, **105**, 104427.
46 M. Orhan Puskullu, B. Tekiner and S. Suzen, *Mini-Rev. Med. Chem.*, 2013, **13**, 365–372.
47 E. A. Wilhelm, A. T. Ferreira, M. P. Pinz, A. S. Dos Reis, A. G. Vogt, A. L. Stein, G. Zeni and C. Luchese, *An. Acad. Bras. Cienc.*, 2017, **89**, 457–467.
48 M. Sankaran, C. Kumarasamy, U. Chokkalingam and P. S. Mohan, *Bioorg. Med. Chem. Lett.*, 2010, **20**, 7147–7151.
49 S. Dall'Acqua, R. Cervellati, M. C. Loi and G. Innocenti, *Food Chem.*, 2008, **106**, 745–749.
50 D.-O. Kim, Y. L. Chang and C. Y. Lee, *Crit. Rev. Food Sci. Nutr.*, 2004, **44**, 253–273.
51 K. Acosta-Quiroga, C. Rojas-Peña, L. S. Nerio, M. Gutiérrez and E. Polo-Cuadrado, *RSC Adv.*, 2021, **11**, 21926–21954.
52 I. Gülçin and A. Dastan, *J. Enzyme Inhib. Med. Chem.*, 2007, **22**, 685–695.
53 F. Sonmez, Z. Gunesli, B. Z. Kurt, I. Gazioglu, D. Avci and M. Kucukislamoglu, *Mol. Diversity*, 2019, **23**(4), 829–844.
54 C. A. Lipinski, F. Lombardo, B. W. Dominy and P. J. Feeney, *Adv. Drug Delivery Rev.*, 2001, **46**, 3–26.
55 A. Daina, O. Michielin and V. Zoete, *Sci. Rep.*, 2017, **7**, 42717.
56 F. H. Allen, O. Kennard, D. G. Watson, L. Brammer, A. G. Orpen and R. Taylor, *J. Chem. Soc., Perkin Trans. 2*, 1987, S1–S19.
57 D. Cremer, *Acta Crystallogr., Sect. B: Struct. Sci.*, 1984, **40**, 498–500.
58 J. Bernstein, R. E. Davis, L. Shimoni and N.-L. Chang, *Angew. Chem., Int. Ed. Engl.*, 1995, **34**, 1555–1573.

59 G. L. Ellman, K. D. Courtney, V. Andres and R. M. Featherstone, *Biochem. Pharmacol.*, 1961, **7**, 88–95.
60 W. Brand-Williams, M. E. Cuvelier and C. Berset, *LWT-Food Sci. Technol.*, 1995, **28**, 25–30.
61 S. Khwaja, K. Fatima, M. Hasanain, C. Behera, A. Kour, A. Singh, S. Luqman, J. Sarkar, D. Chanda, K. Shanker, A. K. Gupta, D. M. Mondhe and A. S. Negi, *Eur. J. Med. Chem.*, 2018, **151**, 51–61.
62 Bruker AXS INC, *APEX3, SAINT and SADABS*, Bruker AXS Inc., Madison, Wisconsin, USA, 2016.
63 G. M. Sheldrick, *Acta Crystallogr., Sect. C: Struct. Chem.*, 2015, **71**, 3–8.
64 O. V Dolomanov, L. J. Bourhis, R. J. Gildea, J. A. K. Howard and H. Puschmann, *J. Appl. Crystallogr.*, 2009, **42**, 339–341.
65 A. D. Becke, *J. Chem. Phys.*, 1993, **98**, 5648–5652.
66 C. Lee, W. Yang and R. G. Parr, *Phys. Rev. B: Condens. Matter Mater. Phys.*, 1988, **37**, 785–789.
67 P. J. Stephens, F. J. Devlin, C. F. Chabalowski and M. J. Frisch, *J. Phys. Chem.*, 2002, **98**, 11623–11627.
68 W. J. Hehre, K. Ditchfield and J. A. Pople, *J. Chem. Phys.*, 2003, **56**, 2257.
69 P. Geerlings, F. De Proft and W. Langenaeker, *Chem. Rev.*, 2003, **103**, 1793–1874.
70 M. J. Frisch, G. W. Trucks, H. B. Schlegel, G. E. Scuseria, M. A. Robb, J. R. Cheeseman, G. Scalmani, V. Barone, B. Mennucci, G. A. Petersson, H. Nakatsuji, M. Caricato, X. Li, H. P. Hratchian, A. F. Izmaylov, J. Bloino, G. Zheng, J. L. Sonnenberg, M. Hada, M. Ehara, K. Toyota, R. Fukuda, J. Hasegawa, M. Ishida, T. Nakajima, Y. Honda, O. Kitao, H. Nakai, T. Vreven, J. A. Montgomery Jr., J. E. Peralta, F. Ogliaro, M. Bearpark, J. J. Heyd, E. Brothers, K. N. Kudin, V. N. Staroverov, R. Kobayashi, J. Normand, K. Raghavachari, A. Rendell, J. C. Burant, S. S. Iyengar, J. Tomasi, M. Cossi, N. Rega, J. M. Millam, M. Klene, J. E. Knox, J. B. Cross, V. Bakken, C. Adamo, J. Jaramillo, R. Gomperts, R. E. Stratmann, O. Yazyev, A. J. Austin, R. Cammi, C. Pomelli, J. W. Ochterski, R. L. Martin, K. Morokuma, V. G. Zakrzewski, G. A. Voth, P. Salvador, J. J. Dannenberg, S. Dapprich, A. D. Daniels, O. Farkas, J. B. Foresman, J. V. Ortiz, J. Cioslowski and D. J. Fox, *Gaussian 09, Revision A.08*, Gaussian, Inc., Wallingford CT, 2009.
71 R. A. Friesner, J. L. Banks, R. B. Murphy, T. A. Halgren, J. J. Klicic, D. T. Mainz, M. P. Repasky, E. H. Knoll, M. Shelley, J. K. Perry, D. E. Shaw, P. Francis and P. S. Shenkin, *J. Med. Chem.*, 2004, **47**, 1739–1749.
72 W. L. Jorgensen, D. S. Maxwell and J. Tirado-Rives, *J. Am. Chem. Soc.*, 1996, **118**, 11225–11236.